A Numerical Compaction Model of Overpressuring in Shales

by

Laura A. Keith

Thesis submitted to the Faculty of

Virginia Polytechnic Institute and State University

in partial fulfillment of the requirements of the degree of

MASTER OF SCIENCE

in

Geophysics

APPROVED:

J. D. Rimstidt, Chairman

J. A. Burns

S. C. Eriksson

J. F. Read

J. A. Snoke

December, 1982

Blacksburg, Virginia

ACKNOWLEDGEMENTS

Drs. J. Donald Rimstidt, John Burns, Susan Erikkson, J. Arthur Snoke and J. Fred Read oversaw the project, provided comments and suggestions, and reviewed the manuscript. Drs. Reza Malek-Madani and William Saric were helpful in simplifying and deriving the governing set of mathematical equations. Dr. Michael Williams suggested a numerical scheme to apply to the equations. Ted Johnson reviewed an early version of the manuscript and provided moral support throughout the project. Financial support was given by fellowships from the Atlantic Richfield Company and the Mineral Mining Resource Research Institute.

TABLE OF CONTENTS

LIST OF FIGURES

NOMENCLATURE

a	slope to linear equation of ϕ and κ over small ϕ ranges
A	pre-exponential in smectite-illite Arrhenius equation (exper.: 4.47×10^{7} yr^{-1}; Gulf Coast: 10,000 yr^{-1})
b	intercept to linear equation of ϕ and κ over small ϕ ranges
c	constant relating shale porosity and depth (3.1×10^{-4} m^{-1})
C_1	constant slope to linear equation of ILL and depth (1.348×10^{-4} m^{-1})
C_2	constant intercept to linear equation of ILL(%) and depth (0.2023)
C_3	constant slopes to linear equation of V_{sp} and depth (7.8×10^{-9}, 2.62×10^{-8} m^2 kg^{-1})
C_4	constant intercepts to linear equation of V_{sp} and depth (9.99×10^{-4}, 9.52×10^{-4} m^3 kg^{-1})
D_1	slope of ln(t) and z linear equation (1103 m yr^{-1})
D_2	intercept of ln(t) and z linear equation (-15,007 m)
E_A/R	activation energy in smectite-illite Arrhenius equation (-9834 °K yr^{-1})
g	gravitational acceleration (9.80665 m sec^{-1})
h	moving boundary (base of section)
H	height of highlands
H_0	initial height of highlands

ILL	illite percentage in sediment
K	hydraulic conductivity (= $\kappa\rho g/\mu$)
ℓ	thickness of sedimentary package
ℓ_w	thickness of water in sedimentary package (= $\phi\ell$)
p	fluid (pore) pressure
p_0	fluid pressure at z = 0 (20 bars)
s	thickness of sediment deposited
s'	sedimentation rate
s_∞	total sediment thickness deposited (= $H_0/[1-\phi_0]$) (4000 m)
S	overburden pressure
SM	percent smectite interlayers in mixed layer clays
SM_0	percent smectite interlayers in mixed layer clays at z = 0
t	time
T	temperature
T'	temperature gradient (25°C/km)
T_0	temperature at z = 0 (293.15 °K)
V	volume of fluid
V_{sp}	specific volume fo fluid
v_r	velocity of solid particles
v_w	velocity of fluid
z	depth
γ	hydrostatic pressure gradient (0.097 bar m^{-1})
γ_s	lithostatic pressure gradient (0.230 bar m^{-1})

Δt	time-step
Δz	depth increment (20 m)
ε	rate constant for erosion (3.957×10^{-15} sec^{-1})
κ	permeability
λ	(= fluid pressure/lithostatic pressure)
μ	dynamic fluid viscosity (1 centipoise)
ξ	dummy variable in integral expressions
ρ	density of fluid (986 kg m^{-3})
ρ_r	density of solid particles (2300 kg m^{-3})
σ	effective stress
ϕ	porosity
ϕ_a	adjusted porosity due to fluid generation factors
ϕ_e	equilibrium porosity (= $\phi_0 e^{-cz}$)
ϕ_0	porosity at z = 0 (0.39)
ψ	hydraulic head
$(--)_{ij}$	discretization of continuous function in numerical scheme
$(--)_{sm\text{-}ill}$	with respect to smectite-illite transformation
$(--)_{therm}$	with respect to thermal expansion fo fluids
$(--)_t$	partial derivative with respect to t
$(--)_z$	partial derivative with respect to z

Note: only subscripts t and z refer to partial derivatives.

INTRODUCTION

In young sedimentary basins, nonequilibrium processes prevail and often produce effects which are stable for significant time periods. Overpressured zones well exemplify such metastable departures from equilibrium conditions. They are characterized by higher pore pressures, temperatures and porosities than normally pressured zones. Overpressure, also referred to as abnormal subsurface pressure, geopressure, or excess pore pressure, is defined as fluid pressure in excess of hydrostatic pressure.

Several mechanisms that promote overpressuring have been proposed. Sediment loading is acknowledged as the major cause (Chapman, 1980; Dickinson, 1953). Numerical models (Smith, 1973; Sharp and Domenico, 1976) testify to the importance of rapid sedimentation on overpressuring; however, this mechanism cannot explain the development of overpressured zones at specific depth intervals (e.g., 3 to 5 km in the Gulf Coast region). Aquathermal pressuring has also been suggested as a cause of overpressuring (Barker, 1972). However, because of its continual temperature and pressure dependence, aquathermal pressuring cannot by itself produce the observed overpressured zones. The illite-smectite dehydration reaction occurs within the depth (temperature) range of interest and has been proposed (Powers, 1967; Burst, 1969) to generate sufficient fluid to account for the reported overpressuring. Numerical models presented in the literature have not considered the effect of clay

dehydration, but schematic arguments (Magara, 1975) indicate it to be a secondary motive. Finally, the role of lithostratigraphic sequence is probably the most important control as to the extent and locality of overpressuring. Permeabilities that are typical in sandstones can usually accomodate the removal of excess fluid generated by any of the aforementioned means. Accordingly, overpressuring normally occurs in low permeability units such as shale where relief of excess pressure is impeded. A feedback relationship among several nonlinear motives would seem necessary to maintain overpressuring for large time periods.

A numerical model is presented which is a one-dimensional, single fluid phase representation of compacting clay sediments that duplicates the effects of such nonequilibrium processes in an evolving sedimentary basin. Although this model could be used in several ways, its present application will be to examine proposed mechanisms of overpressuring. The model follows the evolution of pressure, porosity, permeability, and solid particle and fluid velocities within a vertical column of sediments in a subsiding basin. Also, the depth, pressure, and temperature of a selected sediment package is documented as it moves through time. Additional terms are incorporated to mimic fluid generation by clay mineral transformations and the volume changes of water due to temperature and pressure variations. This model, which calculates the physical properties of a compacting clay column, can be combined with rate models for

geochemical processes to predict the diagenetic state of a sedimentary packet throughout its burial history.

THE MODEL

In an evolving sedimentary basin, burial is often so rapid that pore fluids in clay-rich layers cannot escape quickly enough for fluid pressures to remain at hydrostatic equilibrium and for sediments to compact to equilibrium porosities. This process is known as nonequilibrium compaction. Overpressuring is more prevalent in shales than in sandy sediments because of their inherently lower permeabilities. As observed in this study, permeability is the main physical parameter of the sediment that controls the extent of overpressuring.

According to Hubbert and Rubey (1959), the overburden pressure (S) is divided between effective stress (σ) and pore pressure (p):

$$S = \sigma + p \ . \qquad (1)$$

As sediments are added (i.e., S increases), porosities for a particular burial pathway will decrease or remain constant because of the irreversibility of the compaction process (Plumley, 1980). If overpressuring occurs, σ will be lower but porosities higher than if hydrostatic equilibrium were maintained. Using the concept of equilibrium depth (δz), Rubey and Hubbert (1959) have linked pore pressure and porosity (ϕ) in the following relationship:

$$\phi = \phi_0 e^{-c\delta z} \qquad (2)$$

where $$\delta = [\gamma_s-(p-p_0)/z]/(\gamma_s-\gamma) \quad (3)$$

(using notation as in Chapman, 1972). This exponential porosity relation has been observed for equilibrated shales in many geologic regions with the constant, c, unique to each basin or province (e.g., for the Gulf Coast region, $c = 3.1 \times 10^{-4}$ m^{-1} (Magara, 1971)).

As solid material is added to the basin, its thickness will increase. An increase in the porosities of a section due to nonequilibrium compaction will also cause the sediment column to expand. To calculate sediment thickness, and thus, the depth of the basin at any time, the porosity profile and mass of sediment must be known. Because of the interrelationship between porosity and the depth of the basin, the problem is classified as a moving-boundary or Stefan problem. Figure 1 displays the moving-boundary h, which is considered impermeable, and the coordinate system adopted throughout this study.

Master Variables and Governing Equations

Equation (2) and the following laws are used to derive the governing equations for the model:

continuity of fluid $$(\rho v_w \phi)_z = -(\rho\phi)_t \quad (4)$$

continuity of solid $$(\rho_r v_r[1-\phi])_z = -(\rho_r[1-\phi])_t \quad (5)$$

Darcy's law $$(v_w-v_r)\phi = -K\psi_z \quad (6)$$

FIG. 1-Coordinate system used in the model and for all computer runs.

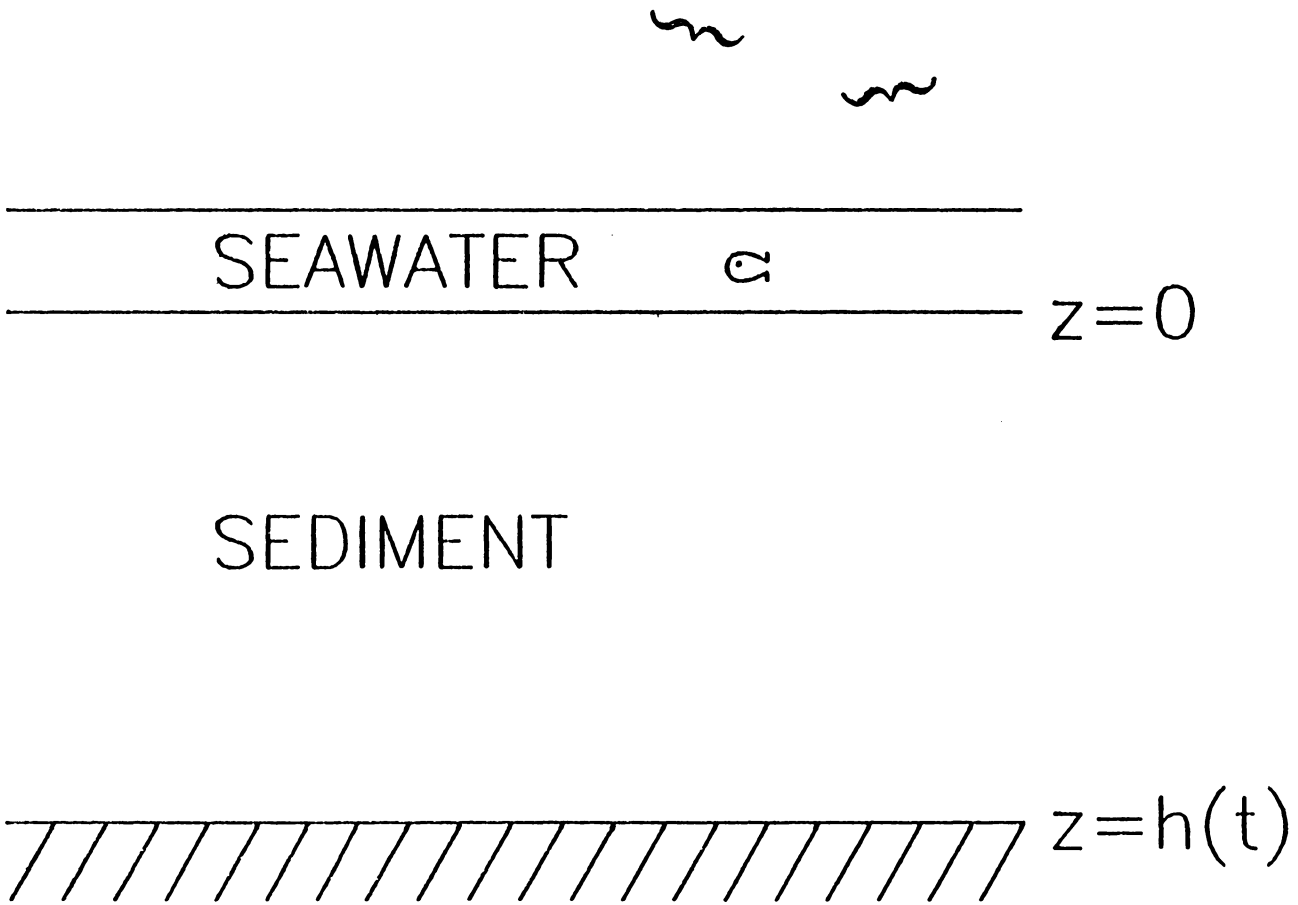
SEAWATER
z=0
SEDIMENT
z=h(t)

(Smith, 1973; Bear, 1972). These equations have been coupled (see Appendix I) resulting in two equations in terms of master variables ϕ and v_r (velocity of the solid particles):

$$B_1\phi_z + B_2[\kappa(\phi)\phi_z/\phi]_z = [\phi_t + v_r\phi_z]/(1-\phi) \qquad (7)$$

$$(v_r[1-\phi])_z = \phi_t \qquad (8)$$

where

$$B_1 = a(\gamma_s-\gamma)/\mu \qquad \text{and} \qquad B_2 = (\gamma_s-\gamma)/\mu c \ .$$

Boundary conditions for ϕ and v_r are either given as specific values or as conditions on their derivatives. At $z = 0$, ϕ is a constant ϕ_0, and v_r is equal to the sedimentation rate ($s'(t)$). Since the lower boundary is impermeable, fluid and solid velocities equalize there. According to Darcy's law, a hydrostatic pressure gradient is preserved, and equation (2) is reduced to the following:

$$\phi_z(h,t) = -c\phi_e(h) \qquad (9)$$

where ϕ_e is the equilibrium porosity value. At $z = h$ the solid velocity is the rate at which the lower boundary h is moving (i.e., subsidence rate). The moving-boundary condition is:

$$v_r(h,t) = h'(t) = [s'(t)(1-\phi_0) + \int_0^h \phi_t(\xi,t)d\xi]/(1-\phi(h,t)) \qquad (10)$$

Adjustments for Fluid Generation Factors

The model includes the effect of fluid volume generated due to the dehydration of smectite to illite and aquathermal pressuring. In computer runs, each of these mechanisms can be considered individually or may be combined. These adjustments are made separately from equations (7) and (8).

Because temperature is not considered in the main equations, the temperature-dependent reaction is taken as a function of depth. In many areas of the Gulf Coast, percentage of illite versus depth can be approximated as a linear function between intervals of 2500 and 4000 m (Freed, 1980; Hower et al,1976) (see Fig. 9):

$$ILL(z) = \begin{cases} C_2 & z < 2500 \text{ m} \\ C_1 z + C_2 & 2500 < z < 4000 \\ C_1(4000) + C_2 & z > 4000 \text{ m}. \end{cases} \qquad (11)$$

Burst (1969) states that the volume of water expelled due to smectite dehydration could be as much as 15% of the compacted bulk volume. The following expression relates volume V and specific volume V_{sp} of the fluid to ϕ:

$$d\phi/\phi = dV/V = dV_{sp}/V_{sp} \ . \qquad (12)$$

If 100% of the smectite in a sedimentary package were to transform, its porosity would increase by 15%; correspondingly:

$$d(ILL)/dz = C_1 \quad \text{and} \quad (d\phi/dz)_{sm\text{-}ill} = C_1 \times 0.15 \; . \qquad (13)$$

The fraction of illite increases as a function of depth alone so a particle must go to a new depth (i.e., one where it has not been before) in order to produce any change in porosity. Therefore, the correction factor $(d\phi/dz)_{sm\text{-}ill}$ depends on the velocity of sedimentary particles (v_r) through the interval 2500-4000 m:

$$(d\phi/dt)_{sm\text{-}ill} = (d\phi/dz)_{sm\text{-}ill} \times v_r \; . \qquad (14)$$

If v_r were negative (directed upward) or zero, the mechanism ceases. To make the adjustment every time-step (Δt), the adjusted porosity (ϕ_a) is given by:

$$\phi_a = \phi_m + (d\phi/dt)_{sm\text{-}ill} \times \Delta t \qquad (15)$$

where ϕ_m is calculated from equation (7). In the example shown later, the amount of smectite which can convert to illite between 2500-4000 m is assumed to be initially 50% of the solids, which is consistent with Gulf Coast compositions (Freed, 1980).

A similar scheme corrects for the volume created due to fluid

expansion. Since density is assumed constant in equations (7) and (8), the following method evaluates the aquathermal effect separately. As observed in overpressured zones (Schmidt, 1973), two different temperature gradients 25°C/km and 40°C/km are used in depth intervals 0-2500 m and 2500-4000 m, respectively. Applying these temperature gradients and a hydrostatic pressure gradient in each depth interval, linear equations expressing specific volume change with depth are derived of the form:

$$V_{sp} = C_3 z + C_4 \quad \text{and} \quad dV_{sp}/dz = C_3 \tag{16}$$

(data taken from Burnham et al, 1969). Rearranging equation (12) and dividing by dz:

$$(d\phi/dz)_{therm} = (\phi/V_{sp}) \times dV_{sp}/dz \ . \tag{17}$$

In the smectite-illite adjustment, the rate of fluid generation is proportional to v_r. Here, rate of fluid expansion or compression depends on the magnitude and direction of v_w:

$$(d\phi/dt)_{therm} = (d\phi/dz)_{therm} \times v_w \ . \tag{18}$$

Adjusted porosity is given as:

$$\phi_a = \phi_m + (d\phi/dt)_{therm} \times \Delta t \ . \tag{19}$$

ASSUMPTIONS AND INPUT PARAMETERS

Assumptions

To derive governing equations (7) and (8) and boundary condition (10) from equations (2) through (6), assumptions concerning physical parameters of the solid, fluid and basin are made. All parameters involved are examined to reveal which ones are important to the problem of overpressuring and also which ones introduce the most mathematical complexity. For example, because the heat flow equation is not solved, certain properties which are temperature dependent are considered constant or a function of depth alone.

The fluid is modeled as incompressible due to the small change in its density (ca. 3%, as calculated from data in Burnham et al (1969)) in the depth range of interest and because thermal expansion of fluids is incorporated as a separate factor. The compressibility of the solids is even smaller so they are also assumed incompressible. Furthermore, even though thermal expansion of water is regarded as a motive for overpressuring, Daines (1982) proposes that the hydraulic conductivity of shale is still sufficient to allow excess fluid to escape over the available time period.

In many models of fluid flow through porous media, viscosity (μ) is held as a unique function of temperature with viscosity decreasing with increasing temperature. For pure water, not contained in a matrix, this relation generally is true. However, in a compacting

sedimentary column, fluid is constrained to flow around clay particles and may become heavily loaded with dissolved solids. Increasing salinity causes viscosity to increase (O'Meara et al, 1971). Assuming a reasonable temperature gradient and depth function for the concentration of sodium chloride (Schmidt, 1973) yields a maximum variation of 0.6 cp over 4 km. Low (1976) has shown that the effective μ of water in montmorillonite increases dramatically as porosity decreases. In most permeability tests, hydraulic conductivity is measured so that this μ increase is taken into account or is made inseparable from the results. Permeability and viscosity are linked to the governing equations only by hydraulic conductivity, expressed in Darcy's law as $K = \kappa\rho g/\mu$. Therefore, variations of viscosity can be balanced in the expression for K by adjusting permeability (κ), where permeability is designed as a unique function of porosity. For modeling purposes, μ is assumed constant with the above variations absorbed by the permeability function.

The base of the column, h, is considered the moving boundary of the system. To reduce the complexity of the boundary conditions, the pressure at the seafloor (p_0) is modeled as constant. Paleobathymetric studies reveal that water depth changes negligibly compared to the thickening of a subsiding basin along passive margins (Hardenbol et al, 1981).

Input Parameters

The main physical parameter that impedes or facilitates fluid flow in sediments is permeability. For typical porous rocks, porosity and permeability are intimately related. Data relating ϕ and κ for different clays, including smectite, illite, kaolinite (Fig. 2B) and shales (Fig. 2A), were gathered from the literature. Because a sound theoretical basis relating permeability and porosity has not been documented, an adequate ϕ-κ function was empirically derived from the sparse data. Sandstones (Chilingarian and Wolf, 1976; Rieke III and Chilingarian, 1974) and some clay minerals (note kaolinite, Fig. 2B) show an approximately linear relationship between porosity and log permeability. For simplicity, a least squares fit of the ϕ-log(κ) linear equation was deduced for each clay (see Appendix II).

Sediments may be deposited on the seafloor at constant or variable rates. Given the rate changes of subsidence along passive margins (Van Hinte, 1978) and of highland erosion, sedimentation rates are likely to decrease exponentially with time. The function used for most computer runs was the following:

$$s'(t) = \varepsilon s_{\infty} e^{-\varepsilon t} \quad . \tag{20}$$

(see Appendix III). Actually, sedimentation may be perturbed by cyclic deposition within a prograding delta system. Equation (20) superimposed on an asymmetric, periodic function would model such cyclic sedimentation.

FIG. 2-Porosity and log permeability points for (A) shales and mudstones and (B) kaolinite as presented in the literature. (Rieke III and Chilingarian, 1974; Wolff, 1982; Bredehoeft and Hanshaw, 1968; Honda and Magara, 1982; Beavis et al, 1982). Dashed lines are the derived linear least squares fits. Since the curve for shales cannot be precisely located because of the wide scatter of points, computer tests were performed to find the optimum function (solid line, Fig. 2A) (see text).

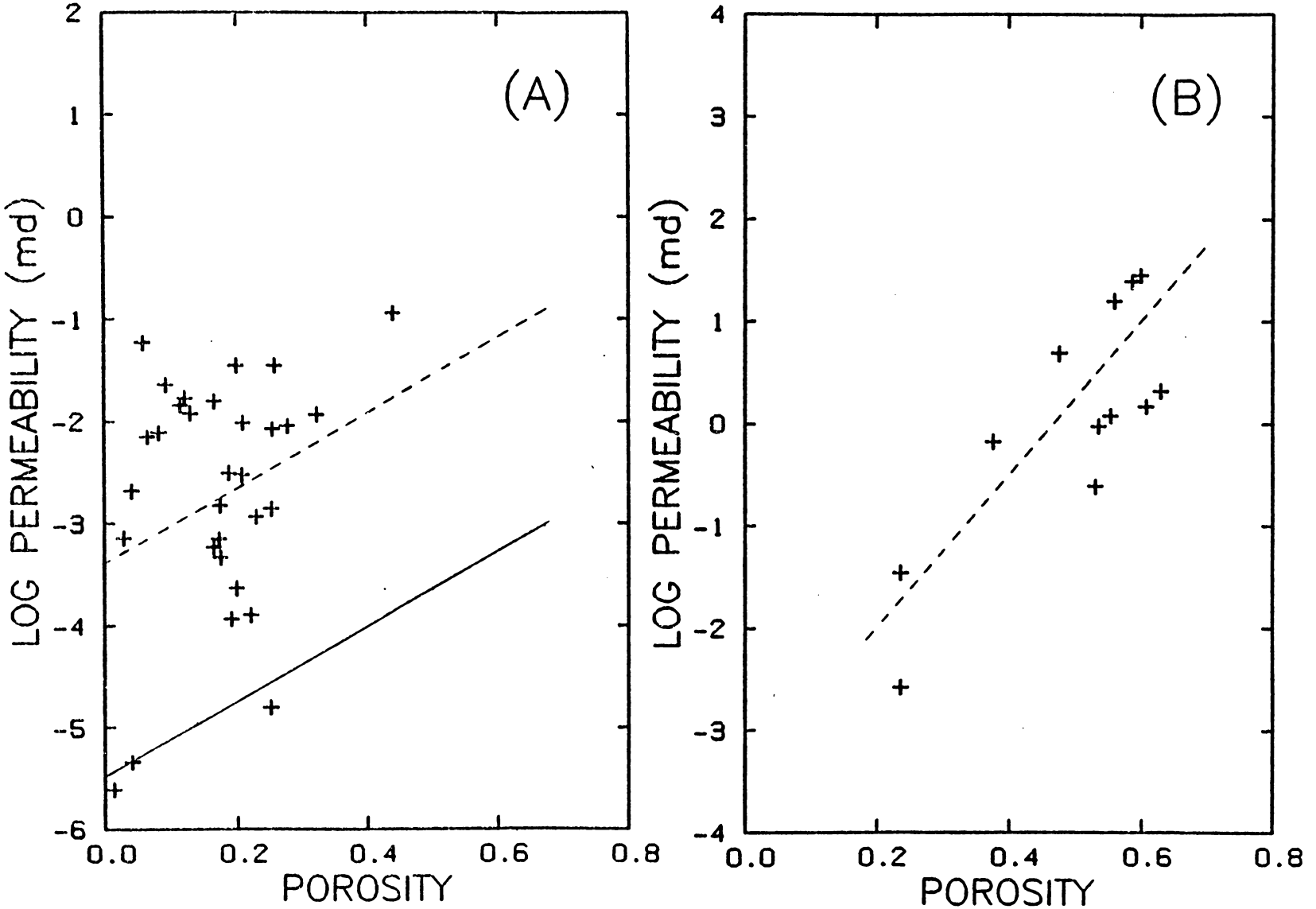
(A)
LOG PERMEABILITY (md)
POROSITY
2
1
0
-1
-2
-3
-4
-5
-6
0.0
0.2
0.4
0.6
0.8
(B)
LOG PERMEABILITY (md)
POROSITY
4
3
2
1
0
-1
-2
-3
-4
0.0
0.2
0.4
0.6
0.8

IMPLEMENTATION OF PROBLEM

Because of the complexity of the problem and the large time spans of interest, extensive computer use was necessary. All computer runs and graphics were performed on an IBM/370 computer system at Virginia Tech (see Appendix IV for computer code). A single computer run extending up to 50 m.y. used approximately 20 CPU minutes and 1 megabyte storage.

Numerical Model

Because ϕ and v_r could not be determined analytically, a numerical method was applied to the governing equations and implemented on the computer. The method used is a mixed explicit-implicit, noniterative finite difference scheme. An explicit scheme involves obtaining the solution at each present point in terms of known preceding and boundary values. Therefore, the size of time-steps is usually a critical stabilizing factor. Implicit schemes provide solutions by simultaneously calculating present values in terms of known preceding and assumed boundary values. (Ames, 1977). Equations (7), (8) and (10) are solved implicitly except that in equation (7) v_r, a ϕ_z and several ϕ's terms are taken from the previous time-step. A description of how the scheme is applied to the governing equations is given in Appendix V. As is typical of implicit schemes, inversion of a matrix is necessary to obtain the master variable ϕ. An L-U (lower-upper) decomposition handles the

inversion. This technique is quicker and more accurate than standard inversion methods but works only for square, tridiagonal matrices (see Johnson and Riess, 1980).

Although the scheme is essentially implicit, small time-steps (Δt) are required to ensure stability. On the other hand, larger time steps shorten computer time. Throughout this report, stability refers to the calculation of pressure values which fall inside of the lithostatic - hydrostatic range. To maximize efficiency the largest Δt that could preserve stability was sought. In this study formal stability criteria for Δt could not be determined because of the complexity of the moving-boundary problem. Alternatively, a series of computer tests established controls on Δt. Over time lapses of tens of million years and sedimentation rates of 1-100 cm/1000 yr, the upper Δt limit was found to be 1000 yr. This increment was used for all further runs.

Permeability Analyses

Stability depends not only on Δt but also on the ϕ-log(κ) function chosen. Computer tests revealed that the only ϕ-κ range which provided sound results for long time periods is on the lower portion of the shale and mudstone graph (near the solid line in Figure 2A). The reported permeabilities of other clays are too high or low, which cause instability to grow rapidly. The acceptable functions have the same slope as the ϕ-log(κ) linear equation for shales except with lower intercepts. A slight change in slope creates instability,

whereas changing the intercept does not. This observation is reasonable because permeability is considered only as a derivative in the main equation.

If sediment were added at low rates (1-5 cm/1000 yr) over a period of 30 m.y., correct permeabilities should produce nearly hydrostatic results. Under these conditions and holding the ϕ-log(κ) slope constant, test runs were performed with a different intercept value in each. In Figure 3 the generated ϕ and κ points are plotted against one another and contoured according to λ (the ratio of fluid pressure to lithostatic pressure). Approximately in the middle of the plot, lower λ values form a trough. The ϕ-log(κ) function which best fits the trough gives minimum overpressuring for the low $s'(t)$ conditions, and thus, appears to be the most geologically reasonable choice.

FIG. 3-Porosity and log permeability points contoured according to λ (fluid pressure/lithostatic pressure), where $\lambda = 0.43$ corresponds to hydrostatic fluid pressure. Points are from several computer runs where $t = 30$ m.y. and $s'(t) = 5$ cm/1000 yr. Dotted area represents the nearly hydrostatic trough.

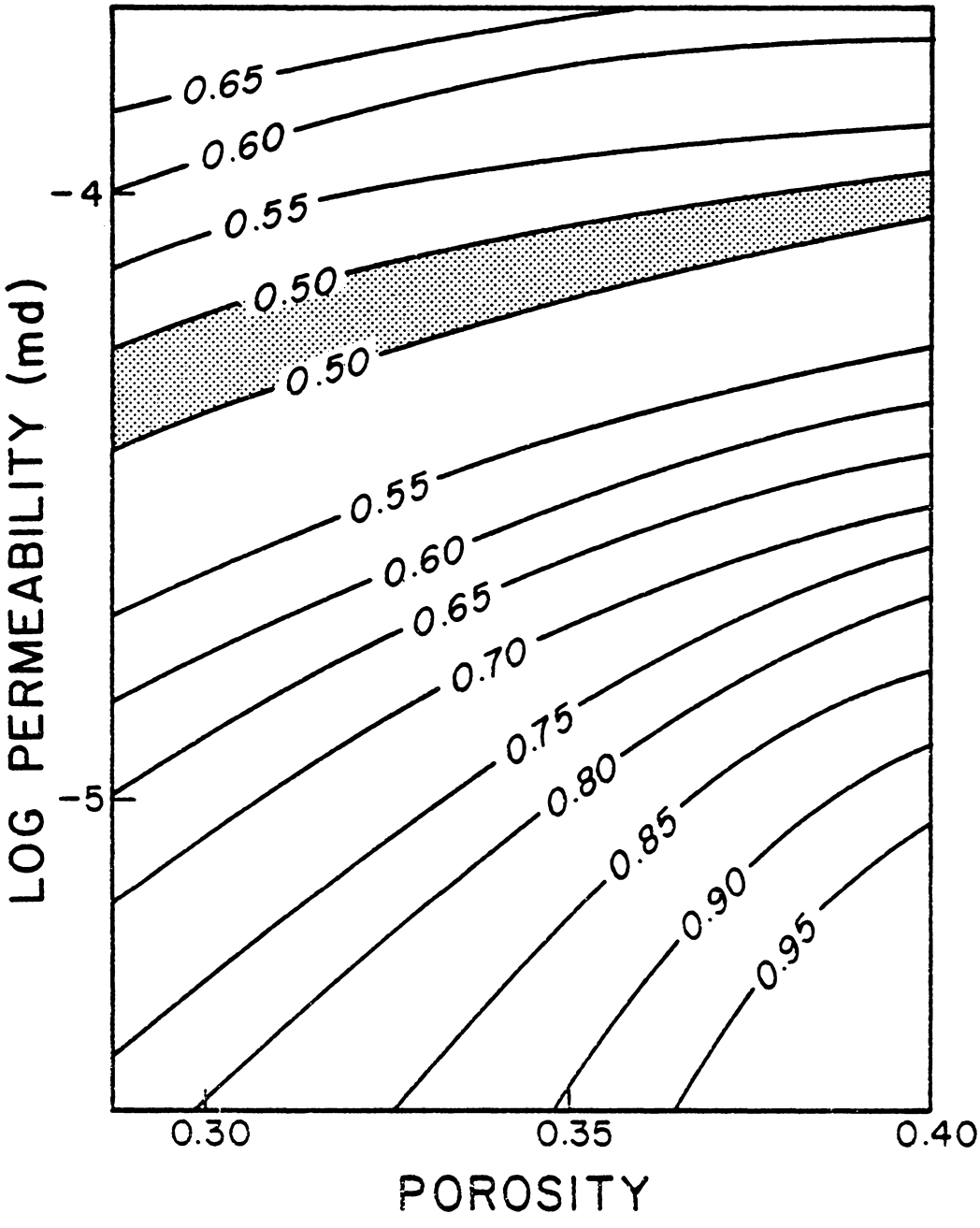
0.65
0.60
0.55
0.50
0.50
0.55
0.60
0.65
0.70
0.75
0.80
0.85
0.90
0.95
-4
-5
LOG PERMEABILITY (md)
0.30
0.35
0.40
POROSITY

DISCUSSION OF RESULTS

Three different cases were run to study their effects on overpressuring:

case I: sediment loading alone (standard)

case II: fluid generation due to smectite-illite transformation and aquathermal pressuring in addition to sediment loading

case III: permeable sediments deposited on shale section.

Figure 4 displays the sedimentation rate curve used. Sedimentation begins as 50 cm/1000 yr and decays rapidly to nearly zero within 40 m.y. This decay is exaggerated beyond what is found for actual basins in order to best illustrate how overpressuring develops and leaks away. Thus, 40 m.y. for this model may correspond to 50 or 60 m.y. in a real basin.

Geological Constraints on Model

The sedimentation represented by the model typifies a passive margin. Stratigraphy may be uncomplicated; therefore, the column can be approximated as composed of shaley sediments or of a regressive sequence of sandstones overlying shales. Cases I and II refer to shale deposition in a continental slope environment, whereas case III represents a deltaic sequence prograding onto marine shales. As in many passive margins, subsidence rates generally decrease

FIG. 4-Sedimentation rate and time curve used in all computer runs

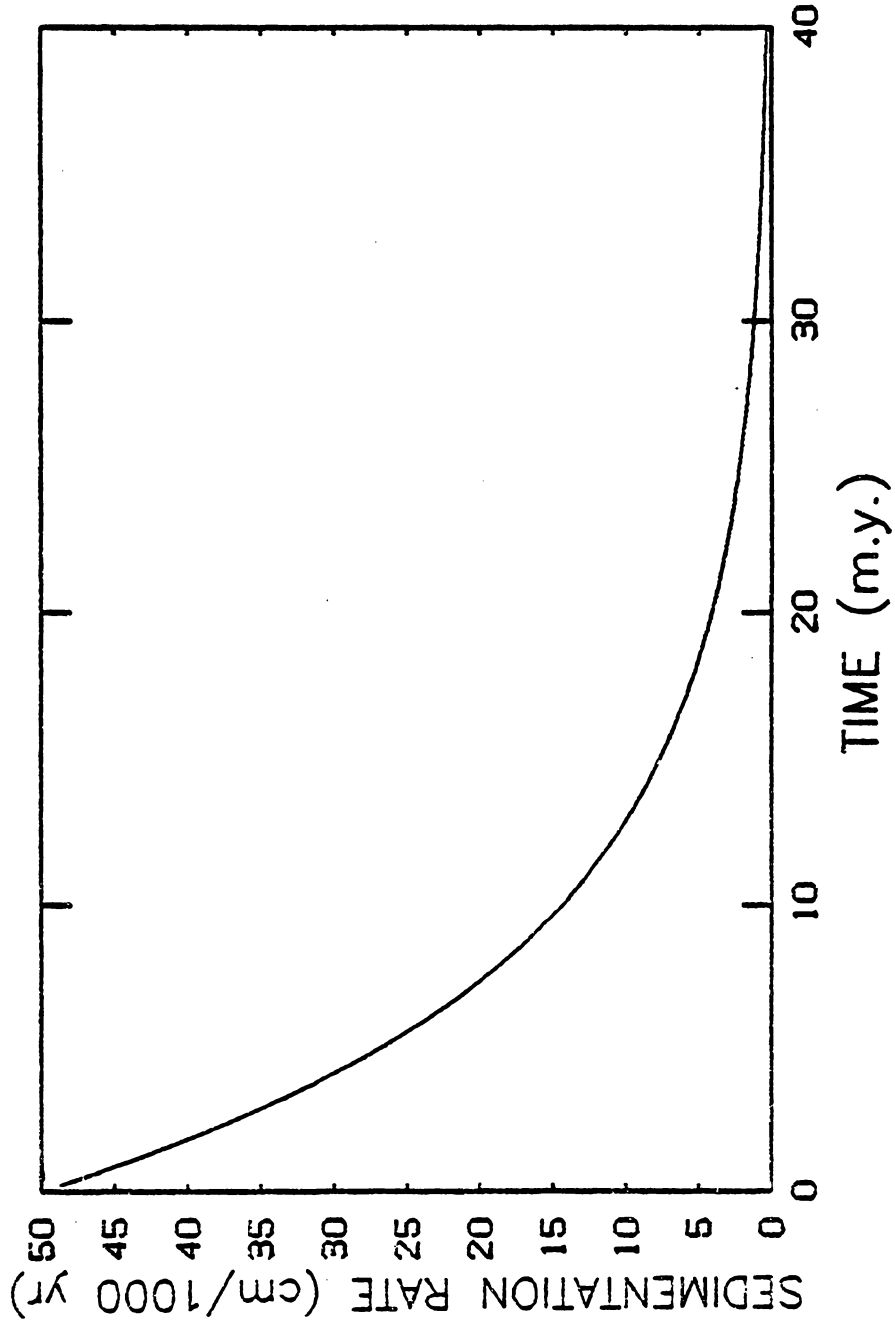
SEDIMENTATION RATE (cm/1000 yr)
0
5
10
15
20
25
30
35
40
45
50
0
10
20
30
40
TIME (m.y.)

exponentially with time (Van Hinte, 1978) and are directly correlated with sediment accumulation. Water depth remains relatively constant as compared to active margins (Hardenbol, Vail and Ferrer, 1981). Faulting along a passive margin may also be uncomplicated, produced only by differential compaction or gravitational mechanisms, such as down-to-basin faulting (e.g., in Gulf Coast basin (Bruce, 1973)). These faults would affect fluid pressures by either acting as conduits for relieving excess fluid or as pressure seals by juxtaposing impermeable and permeable units. Thus, in the presented model, compaction and diagenesis of sedimentary packages are considered without tectonic complications.

The Gulf Coast is a well studied passive margin which has thick shale sections commonly overlain by deltaic sandstone sequences. There are many reported occurrences of overpressuring. Figure 5 displays a typical overpressured section for the Gulf Coast. Instead of forming throughout the section, overpressured zones seem to occur at specific depth intervals correlative to the least permeable horizons. The overpressured shales are generally Oligocene in age, with the overlying sands as young as Pleistocene (Schmidt, 1980). Because of the accessibility of its data, the Gulf Coast will be frequently referred to as a geological comparison.

Cases I and II: Evaluation of Pressure Generation Factors

FIG. 5-Sand percentage and fluid pressure versus depth in Manchester field, Louisiana (modified from Schmidt (1973)). The line with open circles represents the pressure profile, whereas the bar graph represents the sand-to-shale ratio.

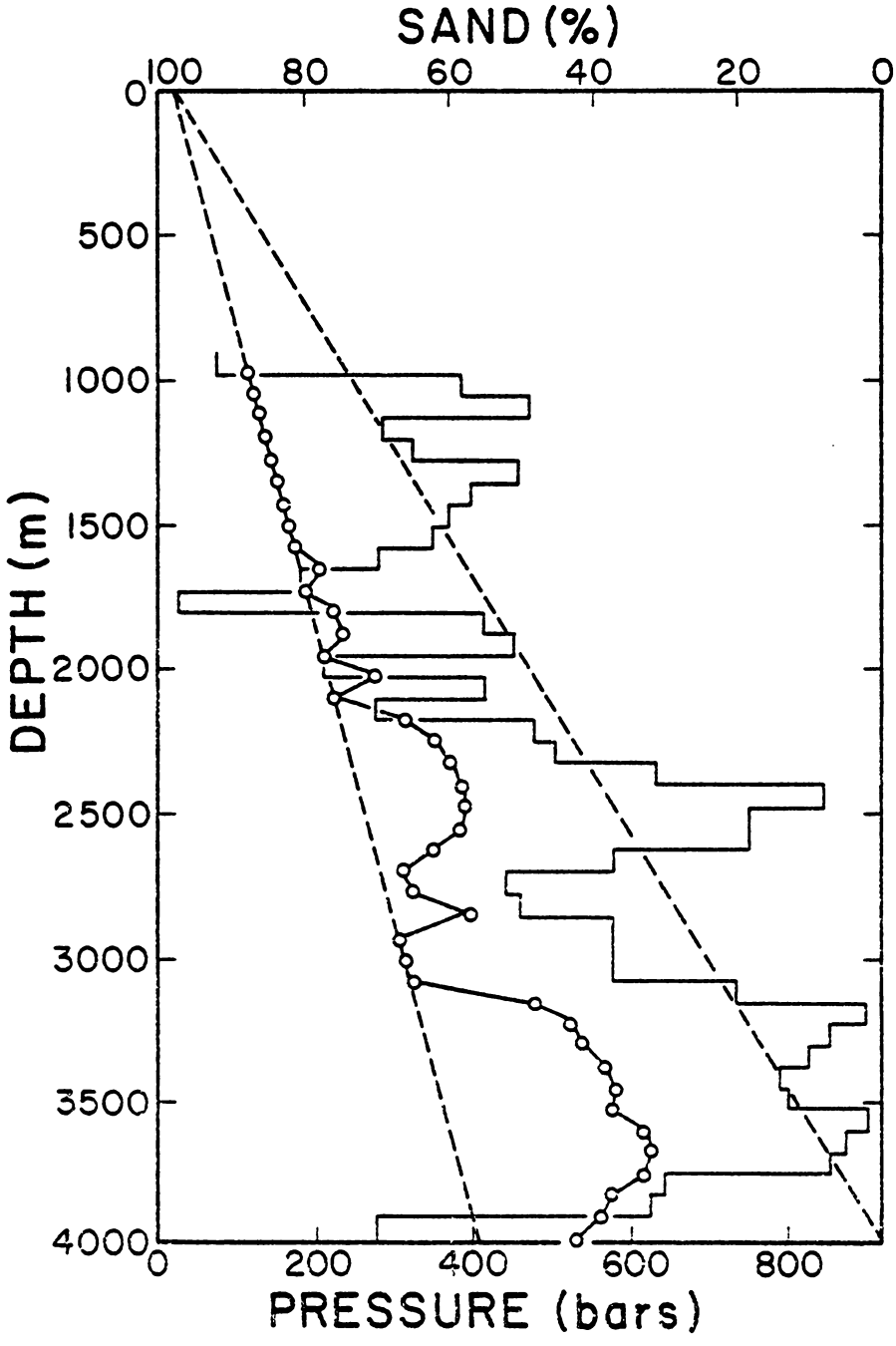
SAND (%)
100
80
60
40
20
0
0
500
1000
1500
2000
2500
3000
3500
4000
DEPTH (m)
0
200
400
600
800
PRESSURE (bars)

In cases I and II clayey sediments comprise the whole section. Pressure and depth are documented every 10 m.y. in Figure 6. Sediment loading causes all the observed overpressuring in case I and a large proportion for case II. Even as early as 10 m.y. (Fig. 6A), fluid which was generated below 2500 m in case II disperses throughout the section, rather than producing a distinct overpressured zone. The pressure curves have maximum divergence at 20 m.y. (Fig. 6B) while sedimentation is still active. In Figures 6C and 6D the curves approach one another and become virtually identical because sedimentation and subsidence have effectively ceased by 30 m.y.

The effects of smectite dehydration and aquathermal pressuring are linked to fluid and solid velocities, and thus, are most important during the active stages of subsidence. Actually, these mechanisms would operate at reduced rates over longer time periods at lower sedimentation rates. Therefore, this model exaggerates their absolute contribution to excess pressure early in the basin's history. At 10 and 20 m.y., though, sediment loading is still the dominant cause of overpressuring. In order to contain the excess pore fluids generated from the the included mechanisms, an impermeable zone must be present at depth to prevent vertical dissipation. This situation would, however, also increase overpressuring due to nonequilibrium compaction, so that the relative contribution of clay dehydration and aquathermal pressuring would still be relatively insignificant. Magara

FIG. 6-Pressure and depth curves for cases I (sediment loading) and II (fluid generation within the section), appropriately labeled, at (A) 10 m.y., (B) 20 m.y., (C) 30 m.y., and (D) 40 m.y.

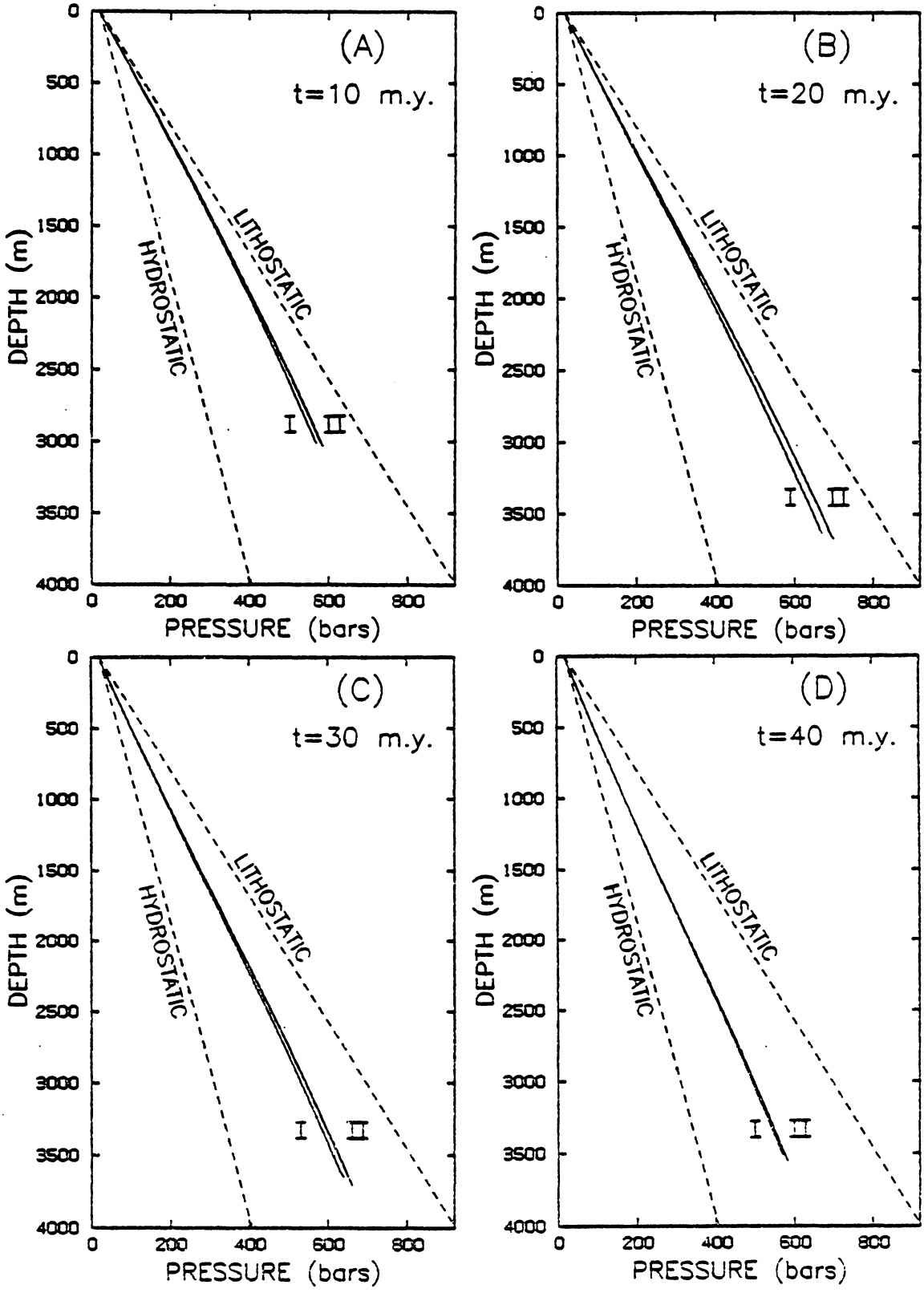
(A)
t=10 m.y.
(B)
t=20 m.y.
(C)
t=30 m.y.
(D)
t=40 m.y.
LITHOSTATIC
HYDROSTATIC
I
II
DEPTH (m)
PRESSURE (bars)
0
500
1000
1500
2000
2500
3000
3500
4000
200
400
600
800

(1975) derives in a schematic fashion similar results for the clay reaction. Daines' (1982) and Chapman's (1980) conclusions support those made here about the secondary effect of thermal expansion.

The pressure curves in Figure 6 differ from those reported in the Gulf Coast basin, as in Figure 5, where distinct overpressured zones form at depth. However, a developing basin composed mostly of shale would show pressure profiles similar to the model's. At 10 m.y. (Fig. 6A) overpressuring dominates the top of the column. As sedimentation rates decline, pressure escapes more rapidly from shallow horizons than from deep ones (Figs. 6C,D). Blatt et al (1980) suggest that overpressuring due to rapid sedimentation facilitates the deformation of shallow sediments by reducing their shear strength. Areas of high sedimentation, such as the Mississippi Delta, commonly show deformation features such as mud lumps, diapiric folds, and general load and slump structures forming at shallow depths because of overpressured, unstable clays (Hanor, 1981). Consequently, soft sediment deformation is symptomatic of these calculated overpressures high in a clay section during and directly following episodes of rapid sedimentation.

Palciauskas and Domenico (1980) state that microfracturing would begin when $\lambda = 0.8$ for systems restraining lateral fluid flow. This limiting value of λ decreases as lateral restraints decrease. At 10 and 20 m.y. microfractures should develop throughout the section, but more extensively in shallow parts. Microfracturing and soft sediment

deformation would tend to relieve excess pressure, especially in the upper part of the sedimentary column, so that at 40 m.y. (Fig. 6D) shallow pressures may approach hydrostatic equilibrium even more closely.

Other numerical models show that rapid sedimentation can cause overpressuring but do not evaluate the effect of clay dehydration or fluid expansion. Smith's compaction model (1973) shows curves resembling those in case I (Fig. 6) when permeabilites similar to the ones in this study are used. Sharp and Domenico (1976) incorporate energy transport but assume more linearized governing equations to produce curves roughly similar to those for case I. Bishop (1979) solves analytically for fluid pressure at depth and also demonstrates the importanance of rapid burial rates on the extent of overpressuring. None of the aforementioned models follow the burial history of sedimentary packages.

Fluid and Sediment Particle Pathways

Fluid and solid velocities for the 2000 m horizon are plotted versus time in Figure 7. Early in the basin's subsidence and sedimentation history, sediment particles and fluid move downward with respect to $z = 0$ (sediment/water interface). However, the magnitude of the solid velocity is greater than for the fluid. Thus, fluid flux is upward with respect to solid particles or stratigraphic markers. Bonham (1980) shows that while sediment is deposited, fluid will be

FIG. 7-Fluid and solid velocities at the 2000 m horizon documented from 10 to 40 m.y. Positive values correspond to flow directed downward relative to the sediment/water interface. Note the times where maximum overpressuring is attained and begins to leaks away and where deflation of the column begins.

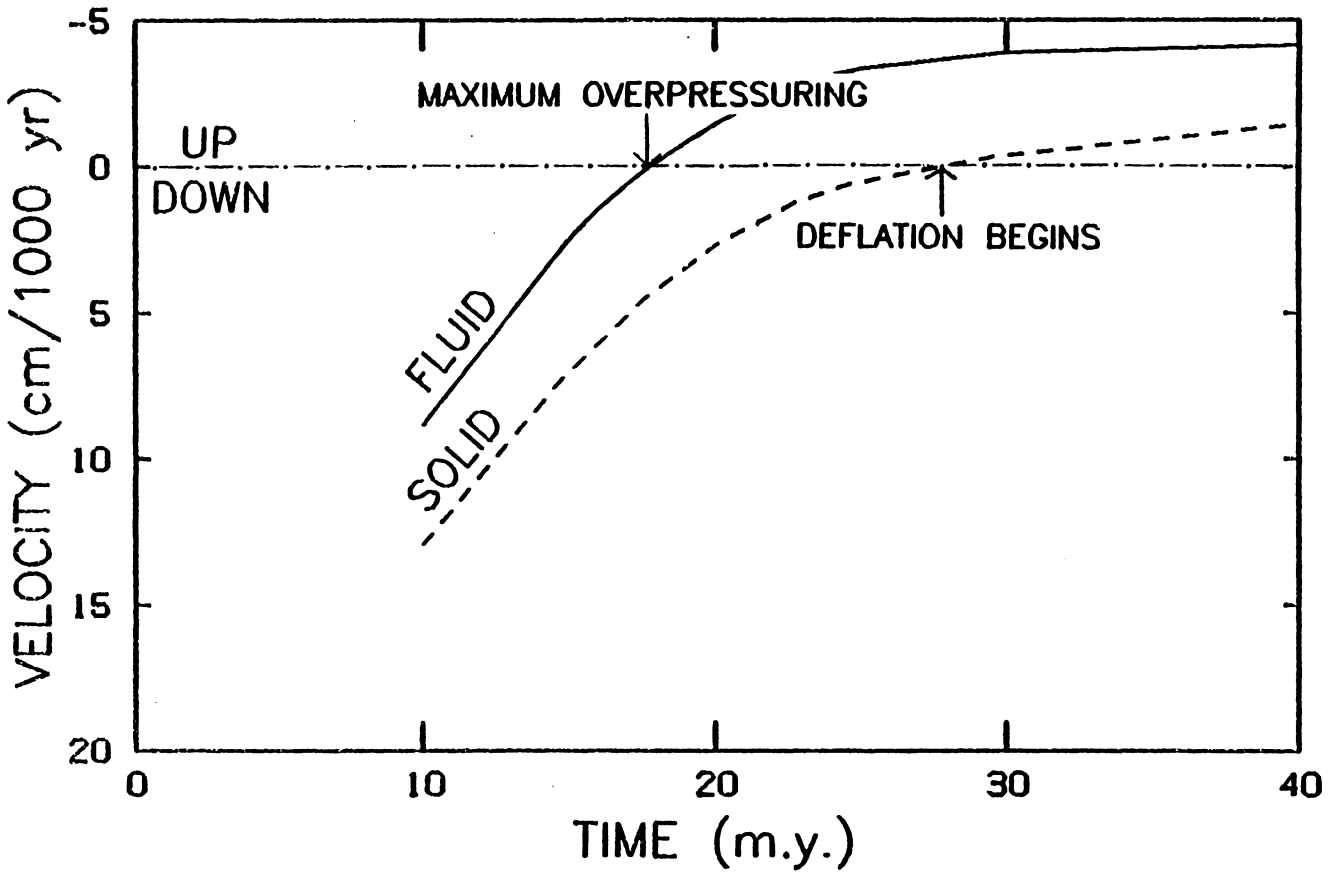
-5
0
5
10
15
20
VELOCITY (cm/1000 yr)
UP
DOWN
MAXIMUM OVERPRESSURING
DEFLATION BEGINS
FLUID
SOLID
0
10
20
30
40
TIME (m.y.)

added to the basin such that absolute fluid velocities are downward. However, if overpressuring develops, this situation may vary. In case I, fluids flow toward the surface once maximum overpressuring is attained and begins to leak away. When the sedimentation rate can no longer keep pace with shrinkage due to waning overpressuring, the whole section deflates (i.e., thickness of basin decreases). Because z = 0 is fixed and z = h is the moving boundary, deflation causes the base of the section to rise in the model. Actually, basin thickness would not decrease because continued sedimentation would fill in the shrinkage gap. Hence, in Figure 7 solid velocities become negative as the column deflates whereas they would remain positive and approach zero when referred to an actual basin. Petroleum will migrate along the same path as the fluid if it is in solution but if it exists as a separate phase it may follow pathways displaced slightly above the fluid's because of the density contrast between hydrocarbons and water.

The pathway of a sedimentary package can be documented through time by calculating how each element in the sedimentary column compacts with each time-step (see Appendix VI). Figure 8A illustrates the burial history of a sedimentary package initially at 200 m depth. Imposing a temperature gradient of 25°C/km transforms the depth curve (Fig. 8A) into a temperature and time plot (Fig. 8B). The age of the sedimentary package as a function of depth shown in Figure 8A, for times less than 25 m.y., can be expressed as:

$$t = e^{[(z-D_2)/D_1]} \quad . \qquad (21)$$

FIG. 8-Burial history of a sedimentary package initially at 200 m depth: (A) depth versus time and (B) temperature versus time.

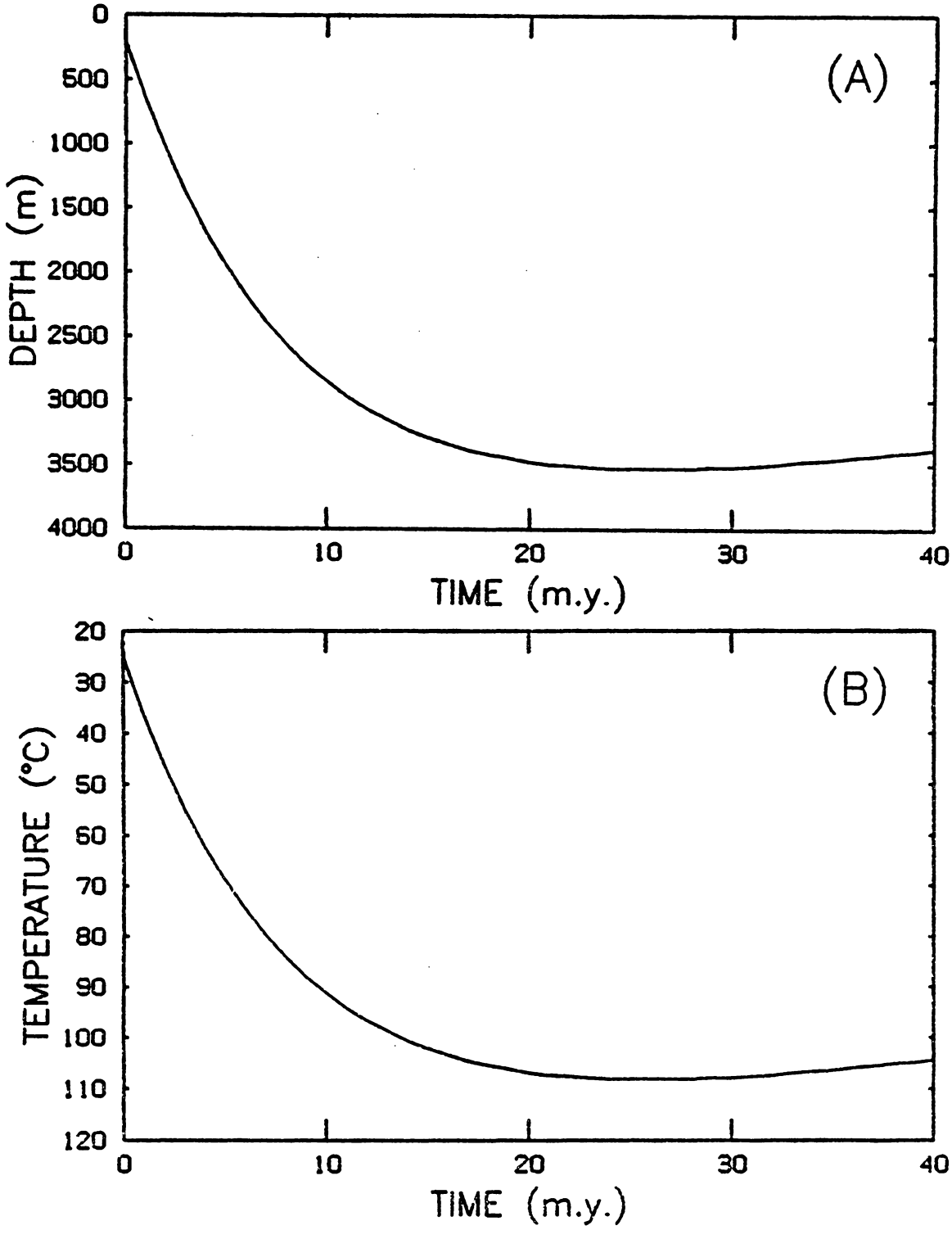
(A)
DEPTH (m)
0
500
1000
1500
2000
2500
3000
3500
4000
0
10
20
30
40
TIME (m.y.)
(B)
TEMPERATURE (°C)
20
30
40
50
60
70
80
90
100
110
120
0
10
20
30
40
TIME (m.y.)

Equation (21) can be directly applied to geochemical rate models to transform them from time to depth dependent.

By combining burial history and rate equations for the smectite to illite transformation (see Eberl and Hower, 1976), the percentage of smectite with depth can be predicted. The intergrated rate equation for the smectite to illite transformation is:

$$\ln[SM/SM_0] = -kt \qquad (22)$$

where k is a function of temperature given by the Arrhenius equation:

$$k = Ae^{(E_A/RT)} \quad . \qquad (23)$$

Combining equations (21), (22), (23) and a temperature gradient yields percentage of smectite layers as a function of depth alone:

$$SM(z) = 0.6\{e^{[-Ae^{\beta}]}\} - 0.2 \qquad (24)$$

where

$$\beta = \{E_A/[R(T'(z)z + T_0)]\} + [(z-D_2)/D_1] \quad . \qquad (25)$$

Because most smectites begin with about 20% illite interlayers and the the main dehydration stage ceases with about 20% smectite layers remaining, this function has been scaled to keep the percent smectite layers in the mixed layer clays between 20 and 80%. Rate constants extrapolated from the experimental results of Eberl and Hower (1976), conducted in a pure potassium system, were directly applied to equation (24) and resulted in the dashed curve shown in Figure 9.

FIG. 9-Percent smectite layers and depth as predicted from the model. Dashed line using rate constants from pure potassium system (Eberl and Hower, 1976). Solid line derived by adjusting the rate constant for inhibition due to the presence of Na^{+}, Ca^{2+}, and Mg^{2+}. Gulf Coast data points from Freed (1980) (circles) and Hower et al (1976) (triangles).

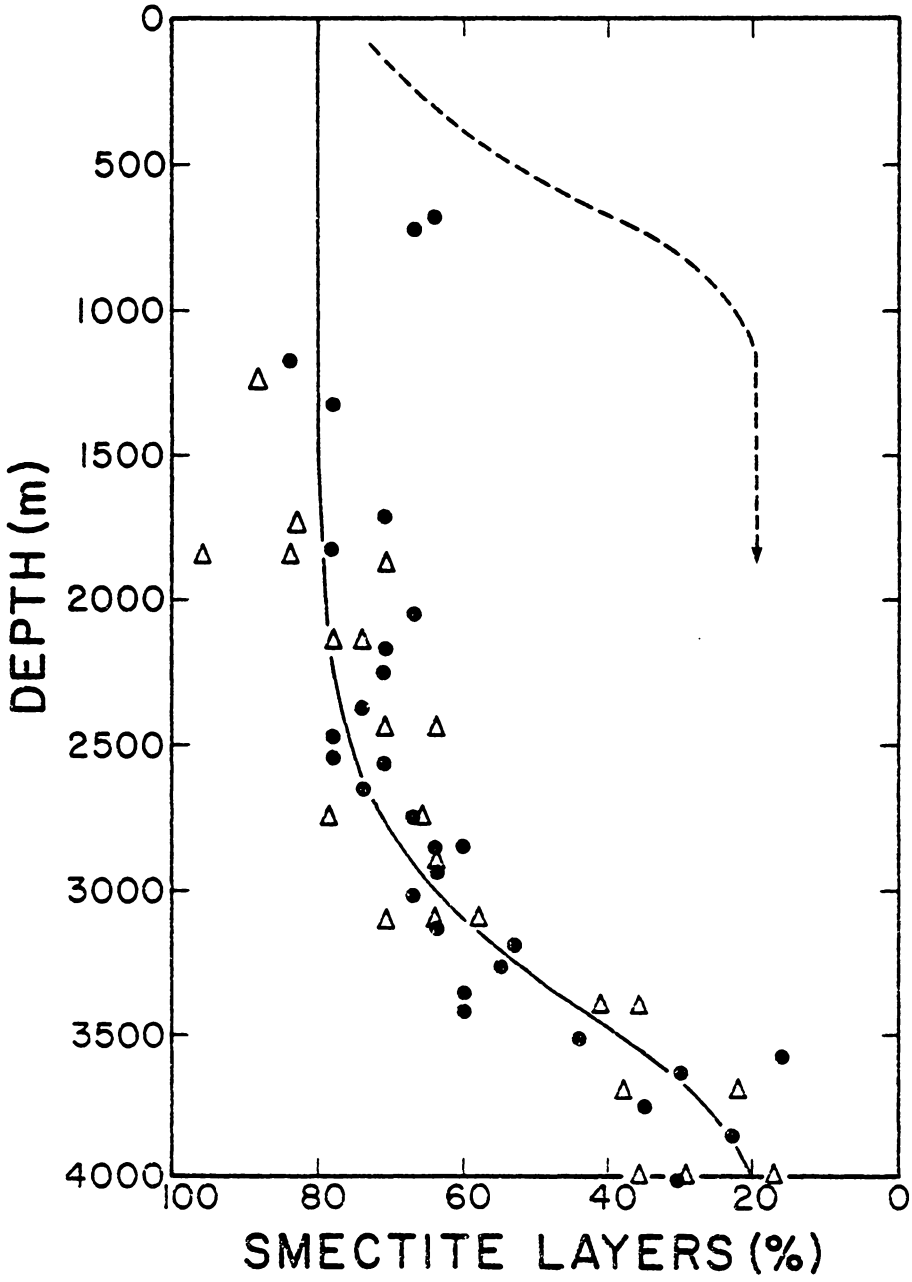
0
500
1000
1500
2000
2500
3000
3500
4000
DEPTH (m)
100
80
60
40
20
0
SMECTITE LAYERS (%)

This curve has the same shape as observed data (note points in Figure 9) but shows the transformation to occur too shallow in the section. The transformation in real shales will be slower than in the pure potassium experiments because Na^{+}, Ca^{2+}, and Mg^{2+} inhibit the transformation of smectite to illite. By lowering the value of A in equation (23) and keeping the activation energy unchanged (i.e., the same reaction mechanism), a percent smectite and depth curve (Fig. 9) is derived which fits much of the Gulf Coast data. Furthermore, the form of the solution (equations (24) and (25)) can be applied to the many diagenetic reactions that follow first order rate laws.

Case III: Lithologic Control on Overpressuring

Because the mechanisms represented in cases I and II do not seem to localize overpressuring to certain depth intervals, the question still remains: why do distinct overpressured zones, like those found in the Gulf Coast (Fig. 5), form? Figure 4 shows that permeability governs the extent of overpressuring. Shales display such a wide range of permeabilities (Fig. 3A) that some may allow the removal of excess pressures faster than others. Sandstones, with even higher permeabilities, rarely show a buildup of excess pressure.

In the Gulf Coast, sandy, deltaic sediments overly thick sequences of marine shales. Overpressuring generally occurs only in the thick shale sections or where the shales and sands intertongue (Dickinson, 1953; Fowler et al, 1971; Schmidt, 1973). Case III was

run to reproduce such observed overpressured profiles. Because the model is designed to mimic only shale compaction, fluid pressures in the overlying sandy sediments are represented simply as hydrostatic. Using the sedimentation curve (Fig. 5), shale was accumulated to 2000 m depth after which 'permeable' (sand rich) sediments were deposited. Figure 10 displays the resulting pressure profiles. The curves closely resemble those seen in the Gulf Coast (Fig. 5), except in the model pressure decays more rapidly. Overpressures, where λ is up to 0.85, are encountered in Oligocene (24-38 m.y.) sediments (Dickinson, 1953; Fowler et al, 1971) whereas the model predicts λ's of 0.7, 0.57, and 0.49 at 20, 30 and 40 m.y., respectively. As stated previously, the sedimentation rate curve was designed to observe how overpressuring develops and leaks away. Actual rates do not decrease as quickly as those here, so overpressuring may be stable for much longer time periods. Also, the presence of permeable units in the section allows excess fluids to escape faster than in a total shale column (Fig. 6).

In case III lithology (permeability) is shown to be an important control of overpressuring. In the model, overpressured zones form at depth where thick shale sections are encountered, as in Gulf Coast sediments (Fig. 5). Many studies of field occurrences support these conclusions. In onshore and offshore Louisiana fields (Schmidt, 1973; Harkins and Baugher, 1969; Fowler et al, 1971), overpressures are reportedly localized in continental slope or deeper marine shales where the sand percentage is less than 10% (Fig. 5). On the other hand,

FIG. 10-Pressure and depth curves for case III at 10, 20, 30 and 40 m.y. Deflection in pressure profile occurs at sand-shale boundary.

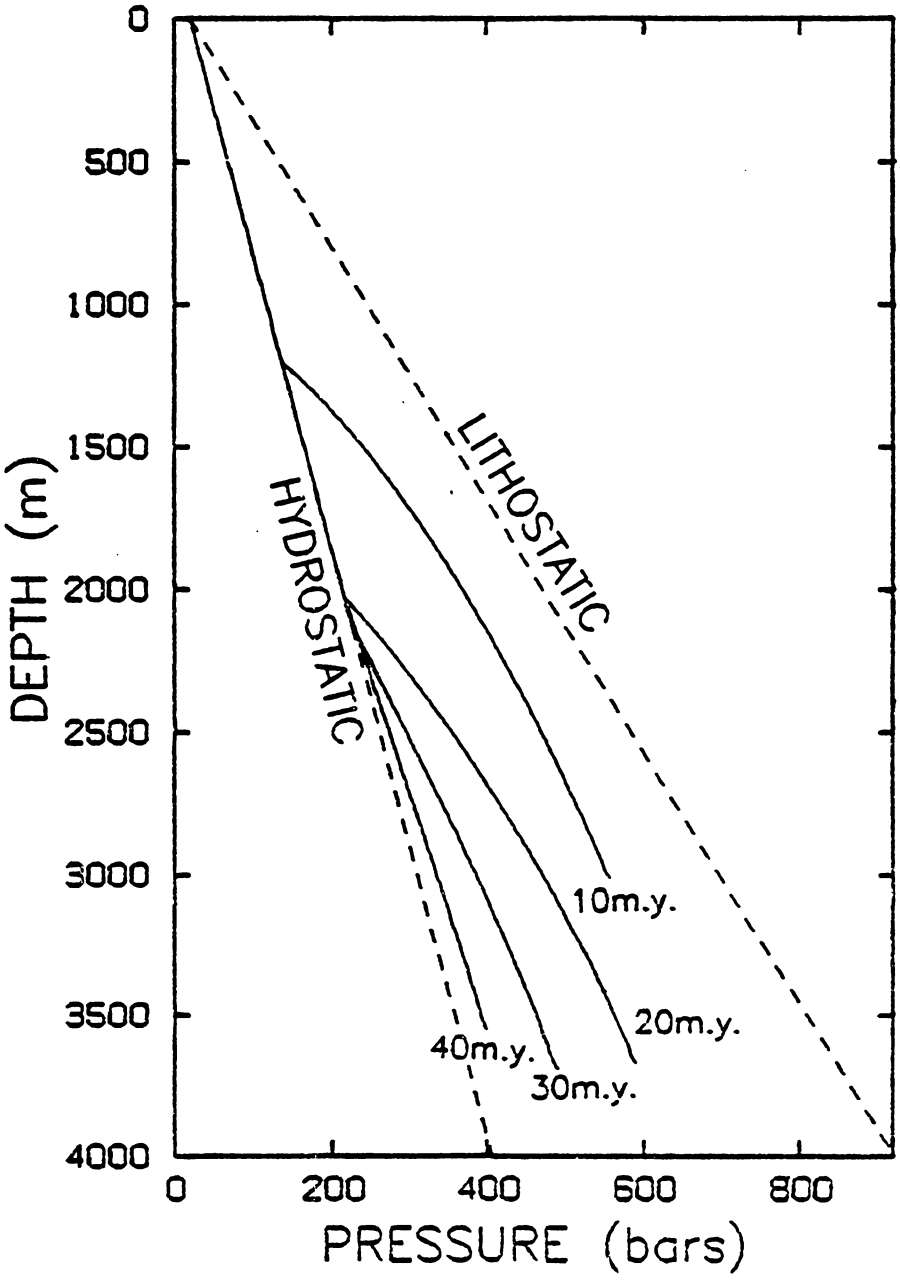
0
500
1000
1500
2000
2500
3000
3500
4000
DEPTH (m)
0
200
400
600
800
PRESSURE (bars)
LITHOSTATIC
HYDROSTATIC
10m.y.
20m.y.
30m.y.
40m.y.

sedimentation rates affect the magnitude and duration of overpressuring, as shown in Figure 10.

SUMMARY AND CONCLUSIONS

The presented numerical model simulates shale compaction in a subsiding sedimentary basin. In the derived system of nonlinear, partial differential equations, master variables are porosity, velocity of solid particles and depth of the evolving basin. They are used to evaluate pressure, fluid velocity, and permeability versus depth at a given time-step or to document the properties of a sedimentary package being successively buried. Because of complexities introduced by the nonlinear equations and moving boundary condition, a numerical scheme was devised which would be stable over tens of million years. Fluid pressure and permeability were found to be directly related. Extensive computer tests reveal a sound relationship between permeability (κ) and porosity (ϕ) for shale as $\log(\kappa) = 3.45\phi - 5.4$ millidarcy.

The following cases were considered to illustrate various controls of overpressuring: (I) simple sediment loading, (II) sediment loading with fluid generation by smectite dehydration and thermal expansion of the aqueous phase, and (III) compaction in a shale section overlain by a highly permeable layer. Cases I and II, in which the column is composed entirely of shale, demonstrate that rapid sedimentation is the dominant cause of overpressuring. Smectite dehydration and aquathermal pressuring produce only minor pressure effects, even considering the low shale permeabilities used in this study. Case III demonstrates the relationship between overpressuring, distribution of

permeabilities through a sedimentary column and age of sediments. That is, overpressuring reaches a higher value and is maintained longer the higher the shale-to-sand ratio is in a section. Field evidence confirms the occurrence of overpressuring in thick shale sequences where the sand percentage is less than 10% (e.g., Figure 5). Also, the appearance of soft sediment deformational features at shallow depths are symptomatic of overpressuring near the top of a shale column during rapid sedimentation, as predicted from cases I and II.

Additional features of evolving sedimentary basins are revealed by these models. During the early stages of subsidence when sedimentation is high, both fluids and solids move downward with respect to the sediment/water interface; however, at all times the fluid moves upward with respect to stratigraphic markers. After maximum overpressuring is attained, fluid migration is upward relative to the sediment/water interface. The depth, pressure, and temperature history of a particular sedimentary package can be documented as it moves through time. This information can be combined with rate models for diagenetic reactions to predict the mineralogy of sediments with depth (e.g., smectite-to-illite ratio).

The presented cases are by no means the only demonstration of the model's capability. A modified model could handle a number of permeability functions so that different lithologic units could be represented. Thus, field cases could be modeled, given good

permeability data. Because of the model's built-in options, diagenesis of actual sedimentary sequences could then be followed, rather than of a hypothetical shale section. A cyclic sedimentation function could be used to see its affect on subsidence curves and the development of overpressuring. Incorporation of energy transport into the model would contribute to attaining the complete burial and diagenetic history of a sedimentary package.

REFERENCES CITED

Ames, W. F., 1977, Numerical methods for partial differential equations: New York, Academic Press, p. 42.

Barker, C., 1972, Aquathermal pressuring - role of temperature in development of abnormal pressure zones: AAPG Bull., v. 56, p. 2068-2071.

Bear, J., 1972, Dynamics fo fluids in porous media: New York, Elsevier, 764 p.

Beavis, F. C., F. I. Roberts, and L. Minskaya, 1982, Engineering aspects of low grade metapelites in an arid climatic zone: Quart. Jour. Eng. Geology London, v. 15, p. 29-45.

Bishop, R. S., 1979, Calculated compaction states of thick abnormally pressured shales: AAPG Bull., p. 918-933.

Blatt, H., G. Middleton, and R. Murray, 1980, Origin of Sedimentary Rocks: Englewood Cliffs, N.J., Prentice-Hall, p. 188-193.

Bonham, L. C., 1980, Migration of hydrocarbons in compacting basins: AAPG Bull., v. 64, p. 549-567.

Bredehoeft, J. D. and B. B. Hanshaw, 1968, On the maintenance of anomolous fluid pressures: I. Thick sedimentary sequences: Geol. Soc. America Bull., v. 79, p. 1097-1106.

Bruce, C. H., 1973, Pressured shale and related sediment deformation: mechanism for development of regional contemporaneous faults: AAPG Bull., v. 57, p. 878-886.

Burnham, C. W., J. R. Holloway, and N. F. Davis, 1969, Thermodynamic properties of water to 1000°C and 10,000 bars: Geol. Soc. America Special Paper, no. 132, 96 p.

Burst, J. F., 1969, Diagenesis of Gulf Coast clayey sediments and its possible relation to petroleum migration: AAPG Bull., v. 53, p. 73-93.

Chapman, R. E., 1972, Primary migration of petroleum from clay source rocks: AAPG Bull., v. 56, p. 2185-2191.

_____, 1980, Mechanical versus thermal cause of abnormally high pore pressure in shales: AAPG Bull., v. 64, p. 2179-2183.

Chilingarian G. V. and K. H. Wolf, 1976, Compaction of coarse-grained sediments, II, in Developments in sedimentology 18b: New York, Elsevier, p. 225-355.

Daines, S. R., 1982, Aquathermal pressuring and geopressure evaluation: AAPG Bull., v. --, p. 931-939.

Dickinson, G., 1953, Geological aspects of abnormal reservoir pressures in Gulf Coast Louisiana: AAPG Bull., v. 37, p. 410-432.

Eberl, D. and J. Hower, 1976, Kinetics of illite formation: Geol. Soc. America Bull., v. 87, p. 1326-1330.

Fowler, et al, 1971, Abnormal pressures in Midland field, Louisiana, in Abnormal subsurface pressure: a study group report: Houston Geol. Soc., p. 48-77.

Freed, R. L., 1980, Shale mineralogy of the no. 1 Pleasant Bayou geothermal test well: a progress report, in Proceedings of the fourth geopressured-geothermal energy conference: Univ. Texas, Austin, p. 153-165.

Hanor, J. S., 1981, Composition of fluids expelled during compaction of Mississippi delta sediments: Geo-Marine Letters, v. 1, p. 169-172.

Hardenbol, J., P. R. Vail, and J. Ferrer, 1981, Interpreting paleoenvironments, subsidence history and sea-level changes of passive margins from seismic and biostratigraphy: Oceanologica Acta, v. 4, p. 33-44.

Harkins, K. L. and J. W. Baugher, 1968, Geological Significance of abnormal formation pressures: Jour. Petroleum Technology, v. 21, p. 961-966.

Honda, H. and K. Magara, 1982, Estimation of irreducible water saturation and effective pore size of mudstones: Jour. Petroleum Geology, v. 4, p. 407-418.

Hower, J. et al, 1976, Mechanism of burial metamorphism of argillaceous sediment: 1. Mineralogical an chemical evidence: Geol. Soc. America Bull., v. 87, p. 725-737.

Hubbert, M. K. and W. W. Rubey, 1959, I. Mechanics of fluid filled porous solids and its application to overthrust faulting: Geol. Soc. America Bull., v. 20, p. 115-164.

Johnson, L. W. and R. D. Riess, 1982, Numerical Analysis: Reading MA, Addison-Wesley, p. 32-41.

Magara, K., 1971, Permeability considerations in generation of abnormal pressures: Soc. Petroleum Eng. Jour., v. --, p. 236-242.

_____, 1975, Reevaluation of montmorillonite dehydration as a cause of abnormal pressure and hydrocarbon migration: AAPG Bull., v. 59, p. 292-302.

Low, P. F., 1976, Viscosity of interlayer water in montmorillonite: Soil Sci. Soc. America Jour., v. 40, p. 500-505.

O'Meara, J. W. et al , ed., 1971, Saline water conversion engineering data book: Piscataway, N. J., M. W. Kellogg, p. OSW-12.90.

Palciauskas, V. V. and P. A. Domenico, 1980, Microfracture development in compacting sediments: relation to hydrocarbon-maturation kinetics: AAPG Bull., v. 64, p. 927-937.

Plumley, W. F., 1980, Abnormally high fluid pressure: survey of some basic principles: AAPG Bull., v. 64, p. 414-430.

Powers, M. C., 1967, Fluid-release mechanisms in compacting marine mudrocks and their importance in oil exploration: AAPG Bull., v. 51, p. 1240-1254.

Rieke ,III, H. H. and G. V. Chilingarian, 1974, Compaction of argillaceous sediments, in Developments in sedimentology 16: New York, Elsevier, p. 142.

Rubey, W. W. and M. K. Hubbert, 1959, Role of fluid pressure in mechanics of overthrust faulting: Geol. Soc. America Bull., v. 70, p. 167-206.

Schmidt, G. W., 1973, Interstitial water composition and geochemistry of deep Gulf Coast shales and sandstones: AAPG Bull., v. 57, p. 321-337.

Sharp, J. M. and P. A. Domenico, 1976, Energy transport in thick sequences of compacting sediment: Geol. Soc. America Bull., v.87, p. 390-400.

Smith, J. E., 1973, Shale compaction: Soc. Petroleum Technology, v. 13, p. 12-22.

Van Hinte, J. E., 1978, Geohistory analysis - application of micropaleontology in exploration geology: AAPG Bull., v. 62, p. 201-222.

Wolff, R. G., 1982, Physical properties of rocks - porosity, permeability, distribution coefficients and dispersivity: U. S. G. S. Open File Report 82-166, 118 p.

APPENDIX I

Derivation of Main Equations

The following continuity relations are derived in Smith (1971):

$$(\rho v_w \phi)_z = -(\rho\phi)_t \tag{4}$$

$$(\rho_r v_r[1-\phi])_z = -(\rho_r[1-\phi])_t \ . \tag{5}$$

If the fluid and solid are assumed incompressible, equations (4) and (5) reduce to:

$$(v_w\phi)_z = -\phi_t \quad \text{and} \quad (v_r[1-\phi])_z = \phi_t \ , \tag{I.1}$$

and rearranging,

$$([v_w - v_r]\phi)_z = -(v_r)_z \tag{I.2}$$

Darcy's law in a system where the solid is moving in respect to the coordinate axes is expressed as

$$(v_w - v_r)\phi = -K\psi_z \ . \tag{I.3}$$

(Bear, 1962). Hydraulic head ψ is derived ignoring the kinetic head term because of the very low velocities involved:

$$\psi = \int_z^h d\xi + \int_{p_0}^{p} d\xi/\rho g = h - z + (p-p_0)/\rho g \ . \tag{I.4}$$

Upon differentiating with respect to z, the following is obtained:

$$\psi_z = p_z/\rho g - 1 \ , \tag{1.5}$$

and combining with equation (1.3):

$$(v_w - v_r)\phi = -K(p_z/\rho g - 1) \ . \tag{1.6}$$

Equation (1.6) is substituted into (1.2):

$$-(K[p_z/\rho g - 1])_z = -(v_r)_z \ . \tag{1.7}$$

Expanding equation (1,1):

$$(v_r)_z = \phi_t + (v_r\phi)_z = \phi_t + v_r\phi_z + \phi(v_r)_z \ , \tag{1.8}$$

and finally,

$$(v_r)_z = [\phi_t + v_r\phi_z]/(1-\phi) \ . \tag{1.9}$$

Substituting equation (1.9) into (1.7),

$$-K_z + (Kp_z)_z/\rho g = [\phi_t + v_r\phi_z]/(1-\phi) \ . \tag{1.10}$$

Hydraulic conductivity is defined as $K = \kappa\rho g/\mu$. Since ρ, g, and μ are assumed constant, κ_z only needs to be evaluated. Over small ϕ intervals, such as 2%, κ and ϕ are represented as linearly related:

$$\kappa(\phi) = a\phi - b \quad . \tag{1.11}$$

In other words, the overall κ-ϕ function is defined by many small linear segments. Thus,

$$K_z = a\rho g\phi_z/\mu \quad . \tag{1.12}$$

Equations (2) and (3) show how porosity, depth, and fluid pressure are related:

$$\phi = \phi_0 e^{-c\delta z} \tag{2}$$

where

$$\delta = [\gamma_s - (p-p_0)]/(\gamma_s-\gamma) \quad . \tag{3}$$

In equation (1.10), p needs to be expressed in terms of ϕ:

$$\phi_z = -c\phi(\delta z)_z = c\phi(p_z - \gamma_s)/(\gamma_s-\gamma) \quad , \tag{1.13}$$

and solving for p_z:

$$p_z = (\gamma_s-\gamma)\phi_z/c\phi + \gamma_s \quad . \tag{1.14}$$

Substituting equations (1.11), (1.12) and (1.14) into (1.10):

$$-A_1\phi_z + (\kappa(\phi)[(\gamma_s-\gamma)\phi_z/c\phi + \gamma_s])_z/\mu = [\phi_t + v_r\phi_z]/(1-\phi) \tag{1.15}$$

where

$$A_1 = a\rho g/\mu \quad .$$

Equation (I.15) can be rearranged to result in equation (7) as given in the text:

$$B_1\phi_z + B_2[\kappa(\phi)\phi_z/\phi]_z = [\phi_t + v_r\phi_z]/(1-\phi) \qquad (7)$$

where

$$B_1 = a\gamma_s/\mu - A_1 = a(\gamma_s-\gamma)/\mu \quad \text{and} \quad B_2 = (\gamma_s-\gamma)/\mu c \ .$$

Boundary conditions are given in terms of the master variables ϕ and v_r at $z = 0$ and $z = h$:

$$\text{at } z = 0: \quad \phi(0,t) = \phi_0 \text{ and } v_r(0,t) = s'(t) \ , \qquad (I.16)$$

$$\text{at } z = h: \quad \phi(h,t) = -c\phi_e(h) \text{ and } v_r(h,t) = h'(t) \ . \qquad (I.17)$$

In order to find an expression for the moving boundary condition $h'(t)$, equation (I.1) for the solid is integrated over the thickness h:

$$\int_0^h (v_r[1-\phi])_z \, d\xi = \int_0^h \phi_t(\xi,t) \, d\xi \qquad (I.18)$$

$$v_r(1-\phi)\Big|_0^h = h'(t)[1-\phi(h,t)] - s'(t)[1-\phi_0] = \int_0^h \phi_t(\xi,t) \, d\xi \ , \qquad (I.19)$$

and finally,

$$h'(t) = [s'(t)(1-\phi_0) + \int_0^h \phi_t(\xi,t) \, d\xi]/(1-\phi(h,t)) \ . \qquad (11)$$

An expression for v_r can be similarly derived:

$$v_r(z,t) = [s'(t)(1-\phi_0) + \int_0^z \phi_t(\xi,t) \, d\xi]/(1-\phi) \ . \qquad (I.19)$$

APPENDIX II

Permeability and Porosity: Summary of the Least Squares Equations

The permeabilities and porosities of several clays were gathered from measurements cited in the literature (Rieke III and Chilingarian, 1974; Wolff, 1982; Bredehoeft and Hanshaw, 1968; Honda and Magara, 1982; Beavis et al, 1982). By the method of least squares, linear relationships of ϕ to log(κ) were found:

montmorillonite:	$\log\kappa = 14\phi - 13$
illite:	$\log\kappa = 8.2\phi - 8.1$
kaolinite:	$\log\kappa = 7.2\phi - 3.5$
shale:	$\log\kappa = 3.5\phi - 3.3$
bentonite:	$\log\kappa = 6.5\phi - 8.1$
clay:	$\log\kappa = -13\phi + 4.8$
OVERALL:	$\log\kappa = 7.9\phi - 4.0$

where κ is given in millidarcies and ϕ as a non-percent.

APPENDIX III

Derivation of the Exponential Form for Sediment Accumulation

Sediment accumulation will be reflective of the rates of erosion. It is assumed that highlands, initially of height H_0, erode material which become sediments of porosity ϕ_0 and are deposited into a basin:

$$s = H/(1-\phi_0) \quad . \tag{III.1}$$

If the rate of erosion follows a first order rate law:

$$-dH/dt = \varepsilon H \tag{III.2}$$

such that

$$\int_{H_0}^{H} dH'/H = -\varepsilon \int_0^t dt' \quad , \tag{III.3}$$

$$\ln(H/H_0) = -\varepsilon t \quad , \tag{III.4}$$

and

$$H = H_0 e^{-\varepsilon t} \quad . \tag{III.5}$$

Substituting equation (III.1) into (III.5),

$$s(t) = s_\infty e^{-\varepsilon t} \tag{III.6}$$

where s_∞ represents the total amount of sediment deposited through infinite time ($H_0/[1-\phi_0]$). Sediment accumulation also follows a first order rate law as shown by differentiating equation (III.6):

$$ds/dt = \varepsilon s(t) \quad , \qquad (III.7)$$

sedimentation rate at any time is found by substituting (III.6) into (III.7):

$$s'(t) = \varepsilon s_\infty e^{-\varepsilon t} \quad . \qquad (20)$$

APPENDIX IV

Computer Program

```
C
C     PROGRAM TO CALCULATE PORE PRESSURES, TEMPERATURES, AND POROSITIES
C     IN A EVOLVING SEDIMENTARY BASIN; GEOPRESSURING IS SOUGHT IN
C     IN ORDER TO ESTIMATE THE CONTRIBUTING FACTORS, THICKNESSES, AND
C     LIFETIMES OF THESE ZONES.
C
C
C
C     PRESENT VERSION :  9 NOV  1982
C
C
C     ********QUIT PARAMETERS : EXPLANATION********
C
C     QUIT=1 : TIME = TIMAX
C     QUIT=2 : POROSITY LESS THAN MIN
C     QUIT=3 : POROSITY GREATER THAN MAX
C     QUIT=4 : NEGATIVE PRESSURES
C     QUIT=5 : STEADY STATE
C     QUIT=7 : NODE NO. DECREASE W TIME
C     QUIT=8 : MAX H REACHED (4500 M)
C
C
C
C
      REAL H,IH,HC,MID,M,L
C     NONDIMENSIONALIZED VARIABLES
      COMMON NODES,T0,TIMAX,TIMINC,TGRAD,TGRAD2,ER,TSINC,TS,TEK,
     .   HC,NC,NC2,PGRAD,P0,DENS,VISC,CAP,CAPR,COND,CONDR,TH,IH,
     .   RDENS,PHI0,PHIH,C,PRINT,QUIT,DZ,TT,SED,SEDR,CT,NODE2,TSS,
     .   NFS,NS,TSED,TSUB,TFS,NPO,H,GAM,SGAM,PLINC,PRMAX,VM,
     .   SUBR,TK,VV0,AA,BB,COR,OH,NMC,TEMPC,TEMPC2,PC,NM
      INTEGER PRINT,QUIT,PRMAX
C     ONE-DIMENSIONALIZED VARIABLES
      COMMON Z(225),DWIDE(225),PHIC(225),OPHIC(225),ZZ(225),
     .   P(225),TEMP(225),MID(225),M(225,225),XI1(225),XI2(225),
     .   PHI(225),PERM(225),VEL(225),PH(225),PL(225),PEX(225),
     .   NAME(80),OPHI(225),VR(225),A(225),B(225),ETA1(225),ETA2(225),
     .   CWIDE(225),ZL(225),U(225,225),L(225,225),ETA3(225)
C
      CALL ERRSET(207,256,-1,0,208)
      CALL INPUT
    2 CALL TIME
      CALL PERME
      CALL PORE
      CALL VELR
C
C     MUST CALL VELW AND PRESS IF CALL THERM
C
C     CALL PRESS
C     CALL VELW
C     CALL THERM
C     CALL CLAY
      CALL COMPAC
C
C     SEE IF TIME TO QUIT OR MAKE PRINTOUT
C
```

```
      IF(TT.GE.TIMAX) QUIT=1
      IF(QUIT.GT.0.) GO TO 4
      PT=(TIMINC/10.0)*PRMAX
      IF(TT.LT.PT) GO TO 2
      PT=TIMINC*PRINT
      IF(TT.LT.PT) GO TO 3
    4 CALL STATIC
      CALL PRESS
      CALL VELW
    3 CALL OUTPUT
      IF(QUIT.GT.0) GO TO 1
      GO TO 2
    1 CONTINUE
      STOP
      END
      SUBROUTINE INPUT
C
C     READS INPUT DATA; REFORMATS AND WRITES DATA
C     ALSO INITIALIZES DATA
C
      REAL H,IH,HC,MID,M,L
C     NONDIMENSIONALIZED VARIABLES
      COMMON NODES,T0,TIMAX,TIMINC,TGRAD,TGRAD2,ER,TSINC,TS,TEK,
     .   HC,NC,NC2,PGRAD,P0,DENS,VISC,CAP,CAPR,COND,CONDR,TH,IH,
     .   RDENS,PHI0,PHIH,C,PRINT,QUIT,DZ,TT,SED,SEDR,CT,NODE2,TSS,
     .   NFS,NS,TSED,TSUB,TFS,NPO,H,GAM,SGAM,PLINC,PRMAX,VM,
     .   SUBR,TK,VV0,AA,BB,COR,OH,NMC,TEMPC,TEMPC2,PC,NM
      INTEGER PRINT,QUIT,PRMAX
C     ONE-DIMENSIONALIZED VARIABLES
      COMMON Z(225),DWIDE(225),PHIC(225),OPHIC(225),ZZ(225),
     .   P(225),TEMP(225),MID(225),M(225,225),XI1(225),XI2(225),
     .   PHI(225),PERM(225),VEL(225),PH(225),PL(225),PEX(225),
     .   NAME(80),OPHI(225),VR(225),A(225),B(225),ETA1(225),ETA2(225),
     .   CWIDE(225),ZL(225),U(225,225),L(225,225),ETA3(225)
C
      CALL STIME(ITIME)
      CALL DATE(IMONTH,IDAY,IYEAR)
      WRITE(4,1090) ITIME,IMONTH,IDAY,IYEAR
      READ(3,1000) NAME
      WRITE(4,1005) NAME
      WRITE(4,1010)
C
C     GENERAL DATA
C
      WRITE(4,1015)
      READ(3,1020) NODES,TT,TIMAX,TIMINC,PLINC,TK,NC,NC2
      WRITE(4,1025) NODES,TT,TIMAX,TIMINC,PLINC,TK,NC,NC2
C
C     CORRECTION FACTOR TO CONVERT SEC TO YEARS
C
      COR=(3.1536E+07)
C
C     WRITE NODE ON GPTIME PLOT
C
      WRITE(9,1095) NC
      G=9.80665
      NMC=NC
      NODE2=NC2
      TT=0.
      NS=1
```

```
      ER=(3.964E-15)
      PRINT=1.1
      TSED=0.0
      QUIT=0.0
      PRMAX=1.1
      WRITE(4,1010)
C
C     HEAT CYCLE DATA
C
      READ (3,1029) TGRAD,T0,PGRAD,P0
      WRITE(4,1031) TGRAD,T0,PGRAD,P0
      WRITE(4,1010)
      TGRAD2=.040
C
C     FLUID PROPERTIES
C
      READ(3,1033) VISC,DENS,CAP,COND
      WRITE(4,1040) VISC,DENS,CAP,COND
      VM=1./DENS
      GAM=G*DENS
      WRITE(4,1010)
C
C     SOLID PROPERTIES
C
      READ(3,1035) C,RDENS,SAVG,H,PHI0,PHIH,CAPR,CONDR
      WRITE(4,1050) C,RDENS,SAVG,CAPR,CONDR,H,PHI0,PHIH
      IH=H
      SGAM=G*SAVG
      AA=(SGAM-GAM)/VISC
      BB=(SGAM-GAM)/(VISC*C)
      WRITE(4,1010)
C
C     NODE DIMENSIONS AND INITIAL CONDITIONS
C
      DZ=20.
      WRITE(4,1070)
      DO 2 J=1,NODES
      N=NODES-J+1.
      READ(3,1021) Z(J),DWIDE(J),TEMP(J),PHI(J)
      CWIDE(N)=DWIDE(J)
      ZZ(N)=Z(J)
      OPHIC(N)=PHI(J)
    2 WRITE(4,1075)J,Z(J),DWIDE(J),PHI(J)
      WRITE(4,1010)
C
C     SED AND SUBS RATES
C
    5 READ(3,1055) SEDR
      WRITE(4,1060) SEDR
      VV0=SEDR*(1.-PHI0)
      WRITE(4,1010)
C
C     FLUID AND HEAT SOURCES
C
      RETURN
C
C     FORMAT STATEMENTS FOR SUBROUTINE INPUT
C
 1000 FORMAT(80A1)
 1005 FORMAT(10X,1H*,80A1)
```

```
1010 FORMAT(/10X,117(1H=))
1015 FORMAT(10X,19HINPUT DATA: GENERAL/)
1020 FORMAT(I5,5E10.3,2I5)
1021 FORMAT(5X,4E10.3)
1025 FORMAT(10X,8HNODES:  ,I5,3X,5HT0:  ,E10.3,3X,8HTIMAX:  ,E10.3,3
    .X,9HTIMINC:  ,E10.3,3X,8HPLINC:  ,E10.3,3X,5HTK:  ,E10.3//10X,
    .40HNODES (TO BE DOCUMENTED THROUGH TIME):  ,I5,5X,I5)
1027 FORMAT(3E10.3)
1029 FORMAT(4E10.3)
1031 FORMAT(10X,21HTEMPERATURE ESTIMATES//10X,8HTGRAD:  ,E10.3,3X,
    .8HTEMP0:  ,E10.3,3X,8HPGRAD:  ,E10.3,3X,5HP0:  ,E10.3)
1033 FORMAT(4E10.3)
1035 FORMAT(8E10.3)
1040 FORMAT(10X,16HFLUID PROPERTIES//
    .10X,19H(CONSTANT) VISC:  ,E10.3,3X,7HDENS:  ,E10.3,3X,6HCAP:  ,E1
    .0.3,3X,7HCOND:  ,E10.3)
1050 FORMAT(10X,25HSOLID (MATRIX) PROPERTIES//10X,16H(CONSTANT)  C:  ,
    .E10.3,3X,8HRDENS:  ,E10.3,3X,7HSAVG:  ,E10.3,3X,7HCAPR:  ,E10.3,3X
    .,8HCONDR:  ,E10.3//
    .10X,42H(INITIAL BOUNDARY CONDITIONS)  H (BASE):  ,E10.3,3X,7HPHI0:
    .  ,E10.3,3X,7HPHIH:  ,E10.3)
1055 FORMAT(E10.3)
1056 FORMAT(I5)
1060 FORMAT(10X,37HCONSTANT SEDIMENTATION RATE (IF USED)//18X,7HSEDR:
    .,E10.3/)
1065 FORMAT(20X,3(3X,E10.3))
1070 FORMAT(10X,31HNODE DIMENSIONS & INITIAL CONDS//21X,4HNODE,9X,
    .1HZ,11X,5HDWIDE,6X,8HPOROSITY/)
1075 FORMAT(20X,I5,3(4X,E10.3))
1080 FORMAT(10X,54HTEMPERATURE DEPENDENT PARAMETERS---SINK & SOURCE TER
    .MS//19X,11HTEMPERATURE,4X,11HFLUS(V/S-V),4X,8HHS (J/S)/)
1085 FORMAT(20X,3(4X,E10.3))
1090 FORMAT(10X,9HGP OUTPUT,8X,12HOUTPUT TIME:,2X,I6,6X,12HOUTPUT DATE:
    .,4X,A2,1H-,A2,1H-,A2//)
1095 FORMAT(I5)
     END
     SUBROUTINE TIME
C
C     COMPUTES TIMESTEPPING AND AMOUNT OF SEDIMENT ADDED TO SYSTEM
C     EACH TIMESTEP. FIGURES OUT TEMPORARY BOUNDARY CONDITIONS.
C     TOTAL SEDIMENT ADDED ALSO CALCULATED.
C
     REAL H,IH,HC,MID,M,L
C     NONDIMENSIONALIZED VARIABLES
     COMMON NODES,T0,TIMAX,TIMINC,TGRAD,TGRAD2,ER,TSINC,TS,TEK,
    .   HC,NC,NC2,PGRAD,P0,DENS,VISC,CAP,CAPR,COND,CONDR,TH,IH,
    .   RDENS,PHI0,PHIH,C,PRINT,QUIT,DZ,TT,SED,SEDR,CT,NODE2,TSS,
    .   NFS,NS,TSED,TSUB,TFS,NPO,H,GAM,SGAM,PLINC,PRMAX,VM,
    .   SUBR,TK,VV0,AA,BB,COR,OH,NMC,TEMPC,TEMPC2,PC,NM
     INTEGER PRINT,QUIT,PRMAX
C     ONE-DIMENSIONALIZED VARIABLES
     COMMON Z(225),DWIDE(225),PHIC(225),OPHIC(225),ZZ(225),
    .   P(225),TEMP(225),MID(225),M(225,225),XI1(225),XI2(225),
    .   PHI(225),PERM(225),VEL(225),PH(225),PL(225),PEX(225),
    .   NAME(80),OPHI(225),VR(225),A(225),B(225),ETA1(225),ETA2(225),
    .   CWIDE(225),ZL(225),U(225,225),L(225,225),ETA3(225)
     REAL HN
C
C     ADD TIMESTEP, EXTRA SEDIMENT
C
```

```
      TT=TT+TK
C
C     SEDIMENT RATE FUNCTION (IF USED)
C     SED RATE IS EXPONENTIALLY DECREASING WITH TIME
C
      SEDR=ER*4000.*EXP(-ER*TT)
      SED=SEDR*TK
      VV0=SEDR*(1.-PHI0)
      TSED=TSED+SED
C
C     FIND NUMBER OF NODES IN NEW H
C
      NN=H/DZ
      HN=NN*DZ
      DH=H-HN
C
C     DEPTH DISCRETIZE  NODES
C
      Z(1)=(DZ+SED)/2.
      DWIDE(1)=DZ+SED
      DO 2 J=2,NN
      Z(J)=Z(J-1)+DZ
    2 DWIDE(J)=DZ
C
C     ASK WHETHER TO CREATE MORE NODES
C     AND INVOKE BOUNDARY CONDITIONS
C
      IF(NN.LE.(NODES-1)) GO TO 15
      IF(NN.EQ.NODES) GO TO 4
      IF(NN.GT.(NODES+1.1)) GO TO 5
      NODES=NODES+1.1
      GO TO 4
    5 IF(NN.GT.(NODES+2.1)) GO TO 6
      NODES=NODES+2.1
      PHI(NODES-1)=-C*DZ*PHI0*EXP(-C*Z(NODES-1))+PHI(NODES-2)
      VR(NODES-1)=VR(NODES-2)
      GO TO 4
    6 IF(NN.GT.(NODES+3.1)) QUIT=6
      NODES=NODES+3.1
      PHI(NODES-2)=-C*DZ*PHI0*EXP(-C*Z(NODES-2))+PHI(NODES-3)
      PHI(NODES-1)=-C*DZ*PHI0*EXP(-C*Z(NODES-1))+PHI(NODES-2)
      VR(NODES-2)=VR(NODES-3)
      VR(NODES-1)=VR(NODES-2)
    4 Z(NODES)=Z(NODES-1)+DZ+DH/2.
      DWIDE(NODES)=DH+DZ
      PHI(NODES)=-C*(DZ+DH/2.)*PHI0*EXP(-C*Z(NODES))+PHI(NODES-1)
      VR(NODES)=VR(NODES-1)
      GO TO 21
   15 IF(NN.LT.(NODES-1)) GO TO 16
      NODES=NODES-1.1
      GO TO 4
   16 IF(NN.LT.(NODES-2.1)) GO TO 17
      NODES=NODES-2.1
      GO TO 4
   17 IF(NN.LT.(NODES-3.1)) QUIT=7
      NODES=NODES-3.1
      GO TO 4
   21 PHI(1)=PHI0*EXP(-C*Z(1))
      PHI(2)=PHI0*EXP(-C*Z(2))
      VR(1)=SEDR
```

```
C
C     DOCUMENT PRESENT H BEING USED (PRINTED IN OUTPUT)
C
      OH=H+SED
      PHIH=-(C*(DZ+DH)*PHI0*EXP(-C*OH)/2.)+PHI(NODES)
C
C     CHECK FOR OVERLYING HYDROSTATIC NODES  (SIMULATE SAND BED)
C
C     IF(NMC.GT.50) GO TO 24
C     GO TO 26
C  24 NGP=ZZ(NC2)/DZ
C     DO 25 J=1,NGP
C     PHI(J)=PHI0*EXP(-C*Z(J))
C  25 CONTINUE
C  26 CONTINUE
C
C     PUT PRESENT PHIS IN OLD ARRAY
C
      DO 8 J=1,NODES
      OPHI(J)=PHI(J)
    8 CONTINUE
      RETURN
      END
      SUBROUTINE STATIC
C     CALCULATES HYDROSTATIC AND LITHOSTATIC PRESSURES AT ALL DEPTHS
C     AND TIME INTERVALS.
C     **NOTE: NEED TO CHANGE BEFORE ENTER 'REAL' PRESSURE
C
      REAL H,IH,HC,MID,M,L
C     NONDIMENSIONALIZED VARIABLES
      COMMON NODES,T0,TIMAX,TIMINC,TGRAD,TGRAD2,ER,TSINC,TS,TEK,
     .   HC,NC,NC2,PGRAD,P0,DENS,VISC,CAP,CAPR,COND,CONDR,TH,IH,
     .   RDENS,PHI0,PHIH,C,PRINT,QUIT,DZ,TT,SED,SEDR,CT,NODE2,TSS,
     .   NFS,NS,TSED,TSUB,TFS,NPO,H,GAM,SGAM,PLINC,PRMAX,VM,
     .   SUBR,TK,VV0,AA,BB,COR,OH,NMC,TEMPC,TEMPC2,PC,NM
      INTEGER PRINT,QUIT,PRMAX
C     ONE-DIMENSIONALIZED VARIABLES
      COMMON Z(225),DWIDE(225),PHIC(225),OPHIC(225),ZZ(225),
     .   P(225),TEMP(225),MID(225),M(225,225),XI1(225),XI2(225),
     .   PHI(225),PERM(225),VEL(225),PH(225),PL(225),PEX(225),
     .   NAME(80),OPHI(225),VR(225),A(225),B(225),ETA1(225),ETA2(225),
     .   CWIDE(225),ZL(225),U(225,225),L(225,225),ETA3(225)
C
      DO 1 J=1,NODES
      PH(J)=GAM*Z(J)+P0
      PL(J)=SGAM*Z(J)+P0
    1 CONTINUE
      RETURN
      END
      SUBROUTINE PRESS
C
C     CALCULATES FLUID PRESSURE AT ALL DEPTHS AND TIME
C
C     PRESENT VERSION CALCULATES EXCESS PRESSURES
C
      REAL H,IH,HC,MID,M,L
C     NONDIMENSIONALIZED VARIABLES
      COMMON NODES,T0,TIMAX,TIMINC,TGRAD,TGRAD2,ER,TSINC,TS,TEK,
     .   HC,NC,NC2,PGRAD,P0,DENS,VISC,CAP,CAPR,COND,CONDR,TH,IH,
     .   RDENS,PHI0,PHIH,C,PRINT,QUIT,DZ,TT,SED,SEDR,CT,NODE2,TSS,
```

```
     .   NFS,NS,TSED,TSUB,TFS,NPO,H,GAM,SGAM,PLINC,PRMAX,VM,
     .   SUBR,TK,VV0,AA,BB,COR,OH,NMC,TEMPC,TEMPC2,PC,NM
      INTEGER PRINT,QUIT,PRMAX
C     ONE-DIMENSIONALIZED VARIABLES
      COMMON Z(225),DWIDE(225),PHIC(225),OPHIC(225),ZZ(225),
     .   P(225),TEMP(225),MID(225),M(225,225),XI1(225),XI2(225),
     .   PHI(225),PERM(225),VEL(225),PH(225),PL(225),PEX(225),
     .   NAME(80),OPHI(225),VR(225),A(225),B(225),ETA1(225),ETA2(225),
     .   CWIDE(225),ZL(225),U(225,225),L(225,225),ETA3(225)
C
      DO 1 J=1,NODES
      ARG=PHI(J)/PHI0
      P(J)=(ALOG(ARG)*(SGAM-GAM)/C)+SGAM*Z(J)+P0
      IF(P(J).LE.0.0) QUIT=4
      PEX(J)=P(J)-PH(J)
    1 CONTINUE
      RETURN
      END
      SUBROUTINE PORE
C
C     CALCULATES POROSITY AS A FUNCTION OF PRESSURE
C
      REAL H,IH,HC,MID,M,L
C     NONDIMENSIONALIZED VARIABLES
      COMMON NODES,T0,TIMAX,TIMINC,TGRAD,TGRAD2,ER,TSINC,TS,TEK,
     .   HC,NC,NC2,PGRAD,P0,DENS,VISC,CAP,CAPR,COND,CONDR,TH,IH,
     .   RDENS,PHI0,PHIH,C,PRINT,QUIT,DZ,TT,SED,SEDR,CT,NODE2,TSS,
     .   NFS,NS,TSED,TSUB,TFS,NPO,H,GAM,SGAM,PLINC,PRMAX,VM,
     .   SUBR,TK,VV0,AA,BB,COR,OH,NMC,TEMPC,TEMPC2,PC,NM
      INTEGER PRINT,QUIT,PRMAX
C     ONE-DIMENSIONALIZED VARIABLES
      COMMON Z(225),DWIDE(225),PHIC(225),OPHIC(225),ZZ(225),
     .   P(225),TEMP(225),MID(225),M(225,225),XI1(225),XI2(225),
     .   PHI(225),PERM(225),VEL(225),PH(225),PL(225),PEX(225),
     .   NAME(80),OPHI(225),VR(225),A(225),B(225),ETA1(225),ETA2(225),
     .   CWIDE(225),ZL(225),U(225,225),L(225,225),ETA3(225)
C
C
C     CALCULATE ELEMENTS OF MATRIX M
C
      XI1(1)=(TK/(2.*DWIDE(1)))*(VR(1)+(BB*B(1)*(PHI(1)-1.)/(2.*DWIDE(1)
     .*PHI(1)*PHI(1)))*(PHI(2)-PHI0)+AA*A(1)*(PHI(1)-1.))
      XI2(1)=BB*(TK/(DWIDE(1)*DWIDE(1)))*(PHI(1)-1.)*(A(1)-B(1)/PHI(1))
      NM=NODES-1
      XI1(NODES)=(TK/(2.*DWIDE(NODES)))*(VR(NODES)+(BB*B(NODES)*(PHI(NOD
     .ES)-1.)/(2.*DWIDE(NODES)*PHI(NODES)*PHI(NODES)))*(PHIH-PHI(NM))+AA
     .*A(NODES)*(PHI(NODES)-1.))
      XI2(NODES)=BB*(TK/(DWIDE(NODES)*DWIDE(NODES)))*(PHI(NODES)-1.)*(A(
     .NODES)-B(NODES)/PHI(NODES))
      PHI(1)=(XI1(1)-XI2(1))*PHI0+PHI(1)
      PHI(NODES)=(-XI1(NODES)-XI2(NODES))*PHIH+PHI(NODES)
      DO 2 J=2,NM
      N=J+1.1
      I=J-1.1
      XI1(J)=(TK/(2.*DZ))*(VR(J)+(BB*B(J)*(PHI(J)-1.)/(2.*DZ*PHI(J)*PHI(
     .J)))*(PHI(N)-PHI(I))+AA*A(J)*(PHI(J)-1.))
    2 XI2(J)=BB*(TK/(DZ*DZ))*(PHI(J)-1.)*(A(J)-B(J)/PHI(J))
C
C     ADD OLD PHI VALUES AND BOUNDARY COND MATRIX
C
```

```
C
C     CONSTRUCT MATRIX M
C
      DO 3 J=1,NODES
      IF(J.EQ.1.1) GO TO 4
      M(J,J-1)=XI2(J)-XI1(J)
    4 M(J,J)=1.-2.*XI2(J)
      IF(J.EQ.NODES) GO TO 3
      M(J,J+1)=XI1(J)+XI2(J)
    3 CONTINUE
C
C     LU DECOMPOSITION     M=LU
C
C     DEFINE MATRICES U & L
      U(1,1)=M(1,1)
      U(1,2)=M(1,2)
      L(1,1)=1.
      MID(1)=PHI(1)
      DO 5 J=2,NODES
      L(J,J-1)=M(J,J-1)/U(J-1,J-1)
      L(J,J)=1.
      U(J,J)=M(J,J)-L(J,J-1)*M(J-1,J)
      U(J,J+1)=M(J,J+1)
C
C     LY=B        (L(MID)=PHI)
C
      MID(J)=PHI(J)-L(J,J-1)*MID(J-1)
    5 CONTINUE
C
C     UX=Y         (U(PHI)=MID)
C
      PHI(NODES)=MID(NODES)/U(NODES,NODES)
      DO 6 J=1,NM
      N=NODES-J
      NN=NODES+1.1-J
    6 PHI(N)=(MID(N)-M(N,NN)*PHI(NN))/U(N,N)
C
C     MAKE SURE THAT THE BOUNDARY IS HYDROSTATIC (NEAR 100M)
C
      DO 8 J=1,3
      N=NODES+J-3
      PHI(N)=PHI(N-1)-C*DZ*PHI0*EXP(-C*Z(N))
    8 CONTINUE
      RETURN
      END
      SUBROUTINE THERM
C
C     COMPUTES HOW MUCH POROSITY COULD BE CHANGED DUE TO DENS
C     EXPANSION OF PURE WATER WITH INCREASE TEMP (ALSO INCREASE
C     PRESS EFFECT INCLUDED)
C
      REAL H,IH,HC,MID,M,L
C     NONDIMENSIONALIZED VARIABLES
      COMMON NODES,T0,TIMAX,TIMINC,TGRAD,TGRAD2,ER,TSINC,TS,TEK,
     .   HC,NC,NC2,PGRAD,P0,DENS,VISC,CAP,CAPR,COND,CONDR,TH,IH,
     .   RDENS,PHI0,PHIH,C,PRINT,QUIT,DZ,TT,SED,SEDR,CT,NODE2,TSS,
     .   NFS,NS,TSED,TSUB,TFS,NPO,H,GAM,SGAM,PLINC,PRMAX,VM,
     .   SUBR,TK,VV0,AA,BB,COR,OH,NMC,TEMPC,TEMPC2,PC,NM
      INTEGER PRINT,QUIT,PRMAX
C     ONE-DIMENSIONALIZED VARIABLES
```

```
      COMMON Z(225),DWIDE(225),PHIC(225),OPHIC(225),ZZ(225),
     .   P(225),TEMP(225),MID(225),M(225,225),XI1(225),XI2(225),
     .   PHI(225),PERM(225),VEL(225),PH(225),PL(225),PEX(225),
     .   NAME(80),OPHI(225),VR(225),A(225),B(225),ETA1(225),ETA2(225),
     .   CWIDE(225),ZL(225),U(225,225),L(225,225),ETA3(225)
C
C      ASSUMED DPHI/PHI=DV/V  (ALL EXPANSION IN Z DIRECTION)
C
      DO 1 J=1,NODES
      IF(OH.GT.2500.) GO TO 2
      PHI(J)=PHI(J)*(1.+TK*VEL(J)*(7.8E-09)/VM)
      GO TO 1
    2 PHI(J)=PHI(J)*(1.+TK*VEL(J)*(2.62E-08)/VM)
    1 CONTINUE
      RETURN
      END
      SUBROUTINE CLAY
C
C     COMPUTES HOW MUCH WATER BEING ADDED TO THE SYSTEM FROM
C     THE TRANSFORMATION OF SMECT TO ILL (BY WAY OF ADDING TO PHI)
C
      REAL H,IH,HC,MID,M,L
C     NONDIMENSIONALIZED VARIABLES
      COMMON NODES,T0,TIMAX,TIMINC,TGRAD,TGRAD2,ER,TSINC,TS,TEK,
     .   HC,NC,NC2,PGRAD,P0,DENS,VISC,CAP,CAPR,COND,CONDR,TH,IH,
     .   RDENS,PHI0,PHIH,C,PRINT,QUIT,DZ,TT,SED,SEDR,CT,NODE2,TSS,
     .   NFS,NS,TSED,TSUB,TFS,NPO,H,GAM,SGAM,PLINC,PRMAX,VM,
     .   SUBR,TK,VV0,AA,BB,COR,OH,NMC,TEMPC,TEMPC2,PC,NM
      INTEGER PRINT,QUIT,PRMAX
C     ONE-DIMENSIONALIZED VARIABLES
      COMMON Z(225),DWIDE(225),PHIC(225),OPHIC(225),ZZ(225),
     .   P(225),TEMP(225),MID(225),M(225,225),XI1(225),XI2(225),
     .   PHI(225),PERM(225),VEL(225),PH(225),PL(225),PEX(225),
     .   NAME(80),OPHI(225),VR(225),A(225),B(225),ETA1(225),ETA2(225),
     .   CWIDE(225),ZL(225),U(225,225),L(225,225),ETA3(225)
C
C     MONT TO ILLITE: 15 PERCENT PHI INCREASE
C
      DO 1 J=1,NODES
      IF(Z(J).LT.2500.) GO TO 1
      IF(Z(J).GT.4000.) GO TO 1
      IF(VR(J).LT.0.) GO TO 1
      PHI(J)=PHI(J)+(2.022E-05)*VR(J)*TK
    1 CONTINUE
      RETURN
      END
      SUBROUTINE VELR
C
C     COMPUTES THE VELOCITY OF THE SOLID PARTICLES AT DEPTH POINT.
C     ALSO INCLUDES CALCULATION OF LOWER FREE BOUNDARY 'H'
C
      REAL H,IH,HC,MID,M,L
C     NONDIMENSIONALIZED VARIABLES
      COMMON NODES,T0,TIMAX,TIMINC,TGRAD,TGRAD2,ER,TSINC,TS,TEK,
     .   HC,NC,NC2,PGRAD,P0,DENS,VISC,CAP,CAPR,COND,CONDR,TH,IH,
     .   RDENS,PHI0,PHIH,C,PRINT,QUIT,DZ,TT,SED,SEDR,CT,NODE2,TSS,
     .   NFS,NS,TSED,TSUB,TFS,NPO,H,GAM,SGAM,PLINC,PRMAX,VM,
     .   SUBR,TK,VV0,AA,BB,COR,OH,NMC,TEMPC,TEMPC2,PC,NM
      INTEGER PRINT,QUIT,PRMAX
C     ONE-DIMENSIONALIZED VARIABLES
```

```
      COMMON Z(225),DWIDE(225),PHIC(225),OPHIC(225),ZZ(225),
     .   P(225),TEMP(225),MID(225),M(225,225),XI1(225),XI2(225),
     .   PHI(225),PERM(225),VEL(225),PH(225),PL(225),PEX(225),
     .   NAME(80),OPHI(225),VR(225),A(225),B(225),ETA1(225),ETA2(225),
     .   CWIDE(225),ZL(225),U(225,225),L(225,225),ETA3(225)
C
      SUM=0.0
      DO 1 J=1,NODES
      SUM=DWIDE(J)*(PHI(J)-OPHI(J))+SUM
C
C     CALC ROCK VEL
C
    1 VR(J)=(1./(1.-PHI(J)))*(VV0+SUM/TK)
C
C     CALC FREE BOUNDARY
C
      HC=H
      SUM=SUM-DWIDE(NODES)*(PHI(NODES)-OPHI(NODES))
      H=H+(1./(1.-PHIH))*(TK*VV0+SUM)
C
C     CHECK FOR MAX
C
      IF(H.GE.4500.) QUIT=8
C
C     CALCULATE TOTAL SUBSIDENCE
C
      TSUB=H-IH
      RETURN
      END
      SUBROUTINE VELW
C
C     VELOCITY OF FLUID IS CALCULATED HERE
C     DEFINED BY DARCYS LAW
C
      REAL H,IH,HC,MID,M,L
C     NONDIMENSIONALIZED VARIABLES
      COMMON NODES,T0,TIMAX,TIMINC,TGRAD,TGRAD2,ER,TSINC,TS,TEK,
     .   HC,NC,NC2,PGRAD,P0,DENS,VISC,CAP,CAPR,COND,CONDR,TH,IH,
     .   RDENS,PH10,PHIH,C,PRINT,QUIT,DZ,TT,SED,SEDR,CT,NODE2,TSS,
     .   NFS,NS,TSED,TSUB,TFS,NPO,H,GAM,SGAM,PLINC,PRMAX,VM,
     .   SUBR,TK,VV0,AA,BB,COR,OH,NMC,TEMPC,TEMPC2,PC,NM
      INTEGER PRINT,QUIT,PRMAX
C     ONE-DIMENSIONALIZED VARIABLES
      COMMON Z(225),DWIDE(225),PHIC(225),OPHIC(225),ZZ(225),
     .   P(225),TEMP(225),MID(225),M(225,225),XI1(225),XI2(225),
     .   PHI(225),PERM(225),VEL(225),PH(225),PL(225),PEX(225),
     .   NAME(80),OPHI(225),VR(225),A(225),B(225),ETA1(225),ETA2(225),
     .   CWIDE(225),ZL(225),U(225,225),L(225,225),ETA3(225)
C
      NM=NODES-1
C
C     INVOKE NO FLOW BOUNDARIES
C
      VEL(1)=VR(1)
      VEL(NODES)=VR(NODES)
      DO 1 J=2,NM
C
C     TAKE DERIVATIVE OF P WRT Z
C
      PZ=(P(J+1)-P(J-1))/(Z(J+1)-Z(J-1))
```

```
      VEL(J)=-(PERM(J)/(VISC*PHI(J)))*(PZ-GAM)*VR(J)
    1 CONTINUE
      RETURN
      END
      SUBROUTINE PERME
C
C     CALCULATES PERMEABILITY USED IN PRESENT TIME-STEP
C     IN TERMS OF THE VALUES OF A AND B (LINEAR EQUATIONS ARE MADE
C     EVERY 2% PHI TO FIT OVERALL PERM-PHI FUNCTION)
C
      REAL H,IH,HC,MID,M,L
C     NONDIMENSIONALIZED VARIABLES
      COMMON NODES,T0,TIMAX,TIMINC,TGRAD,TGRAD2,ER,TSINC,TS,TEK,
     .   HC,NC,NC2,PGRAD,P0,DENS,VISC,CAP,CAPR,COND,CONDR,TH,IH,
     .   RDENS,PHI0,PHIH,C,PRINT,QUIT,DZ,TT,SED,SEDR,CT,NODE2,TSS,
     .   NFS,NS,TSED,TSUB,TFS,NPO,H,GAM,SGAM,PLINC,PRMAX,VM,
     .   SUBR,TK,VV0,AA,BB,COR,OH,NMC,TEMPC,TEMPC2,PC,NM
      INTEGER PRINT,QUIT,PRMAX
C     ONE-DIMENSIONALIZED VARIABLES
      COMMON Z(225),DWIDE(225),PHIC(225),OPHIC(225),ZZ(225),
     .   P(225),TEMP(225),MID(225),M(225,225),XI1(225),XI2(225),
     .   PHI(225),PERM(225),VEL(225),PH(225),PL(225),PEX(225),
     .   NAME(80),OPHI(225),VR(225),A(225),B(225),ETA1(225),ETA2(225),
     .   CWIDE(225),ZL(225),U(225,225),L(225,225),ETA3(225)
      DIMENSION AAA(25),BBB(25)
C
C     OVERALL PERME-PHI FUNCTION LOG(PERM)=3.45PHI- 5.4
C
      DATA AAA/ 0.3381E-19,0.3963E-19,0.4645E-19,
     .0.5445E-19,0.6382E-19,0.7481E-19,0.8771E-19,
     .0.1028E-18,0.1205E-18,0.1412E-18,0.1656E-18,
     .0.1941E-18,0.2275E-18,0.2667E-18,0.3126E-18,
     .0.3664E-18,0.4295E-18,0.5035E-18,0.5902E-18,
     .0.6918E-18,0.8110E-18,0.9506E-18,0.1114E-17,
     .0.1306E-17,0.1531E-17/
      DATA BBB/-0.3926E-20,-0.3810E-20,-0.3537E-20,
     .-0.3057E-20,-0.2307E-20,-0.1208E-20,0.3387E-21,
     .0.2452E-20,0.5284E-20,0.9019E-20,0.1389E-19,
     .0.2016E-19,0.2818E-19,0.3837E-19,0.5122E-19,
     .0.6737E-19,0.8756E-19,0.1127E-18,0.1439E-18,
     .0.1825E-18,0.2302E-18,0.2888E-18,0.3609E-18,
     .0.4491E-18,0.5571E-18/
C
      DO 1 J=1,NODES
      IF(PHI(J).LT.(PHIH-.05)) QUIT=2
      IF(PHI(J).GT.PHI0) QUIT=3
      INC=PHI(J)/(0.020)+1
      A(J)=AAA(INC)
      B(J)=BBB(INC)
C
C     CALC PERMEABILITY USED IN THIS TIME STEP
C
    1 PERM(J)=A(J)*PHI(J)-B(J)
      RETURN
      END
      SUBROUTINE COMPAC
C
C     RESETS NODES ACCORDING TO COMPACTION EVERY TIMESTEP
C
C
```

```
      REAL H,IH,HC,MID,M,L
C     NONDIMENSIONALIZED VARIABLES
      COMMON NODES,T0,TIMAX,TIMINC,TGRAD,TGRAD2,ER,TSINC,TS,TEK,
     .   HC,NC,NC2,PGRAD,P0,DENS,VISC,CAP,CAPR,COND,CONDR,TH,IH,
     .   RDENS,PHI0,PHIH,C,PRINT,QUIT,DZ,TT,SED,SEDR,CT,NODE2,TSS,
     .   NFS,NS,TSED,TSUB,TFS,NPO,H,GAM,SGAM,PLINC,PRMAX,VM,
     .   SUBR,TK,VV0,AA,BB,COR,OH,NMC,TEMPC,TEMPC2,PC,NM
      INTEGER PRINT,QUIT,PRMAX
C     ONE-DIMENSIONALIZED VARIABLES
      COMMON Z(225),DWIDE(225),PHIC(225),OPHIC(225),ZZ(225),
     .   P(225),TEMP(225),MID(225),M(225,225),XI1(225),XI2(225),
     .   PHI(225),PERM(225),VEL(225),PH(225),PL(225),PEX(225),
     .   NAME(80),OPHI(225),VR(225),A(225),B(225),ETA1(225),ETA2(225),
     .   CWIDE(225),ZL(225),U(225,225),L(225,225),ETA3(225)
C
C     SEE IF NC2 HAS COME INTO SECTION YET
C     ONLY NEED IF PERM SED.S PRESENT
C
C     IF(NC2.LE.NODES) GO TO 4
C     GO TO 6
C   4 IF(NMC.EQ.NC2) GO TO 6
C     DIF=ZZ(NC)-CWIDE(NC)/2.
C     NN=DIF/DZ
C     NC2=NC+NN
C     NNN=NC+1
C     DO 7 J=NNN,NC2
C     N=NC2-J+1
C     OPHIC(J)=OPHI(N)
C     CWIDE(J)=DZ
C     ZZ(J)=ZZ(J-1)+CWIDE(J)
C   7 CONTINUE
C     CWIDE(NC2)=DZ+(DIF-DZ*NN)
C     ZZ(NC2)=CWIDE(NC2)/2.
C   6 CONTINUE
C     IF(NODES.GE.NODE2) NMC=NC2
C
C     FIND PHI THAT CORRESPONDS TO EACH COMPACTED NODE
C
      DO 3 J=1,NMC
      NZ=1.+ZZ(J)/DZ
    3 PHIC(J)=PHI(NZ)
C
C     FIGURE HOW MUCH BOTTOM NODE COMPACTED
C
      ZL(1)=H
      DELW=-CWIDE(1)*((PHIC(1)-OPHIC(1))/(PHIC(1)-1.0))
      CWIDE(1)=CWIDE(1)+DELW
C
C     FIGURE HOW MUCH REST OF NODES COMPACTED
C
      DO 1 J=2,NMC
      DELW=-CWIDE(J)*((PHIC(J)-OPHIC(J))/(PHIC(J)-1.0))
      CWIDE(J)=CWIDE(J)+DELW
      ZL(J)=ZL(J-1)-CWIDE(J-1)
      ZZ(J)=ZL(J)-CWIDE(J)/2.0
    1 CONTINUE
C
C     PUT PHIS IN OLD ARRAY
C
      DO 5 J=1,NMC
```

```
    5 OPHIC(J)=PHIC(J)
      RETURN
      END
      SUBROUTINE OUTPUT
C     PRINTS OUTPUT (FOR PLOT: SEE GPPLOT FTN DATA ON UNIT 8)
C     EVERY DESIGNATED PRINT TIME STEP.  SCRATCH FILE MADE
C     FOR VALUES THROUGH ALL TIME STEPS.
C
      REAL H,IH,HC,MID,M,L
C     NONDIMENSIONALIZED VARIABLES
      COMMON NODES,T0,TIMAX,TIMINC,TGRAD,TGRAD2,ER,TSINC,TS,TEK,
     .   HC,NC,NC2,PGRAD,P0,DENS,VISC,CAP,CAPR,COND,CONDR,TH,IH,
     .   RDENS,PHI0,PHIH,C,PRINT,QUIT,DZ,TT,SED,SEDR,CT,NODE2,TSS,
     .   NFS,NS,TSED,TSUB,TFS,NPO,H,GAM,SGAM,PLINC,PRMAX,VM,
     .   SUBR,TK,VV0,AA,BB,COR,OH,NMC,TEMPC,TEMPC2,PC,NM
      INTEGER PRINT,QUIT,PRMAX
C     ONE-DIMENSIONALIZED VARIABLES
      COMMON Z(225),DWIDE(225),PHIC(225),OPHIC(225),ZZ(225),
     .   P(225),TEMP(225),MID(225),M(225,225),XI1(225),XI2(225),
     .   PHI(225),PERM(225),VEL(225),PH(225),PL(225),PEX(225),
     .   NAME(80),OPHI(225),VR(225),A(225),B(225),ETA1(225),ETA2(225),
     .   CWIDE(225),ZL(225),U(225,225),L(225,225),ETA3(225)
      TTP=TT/COR
      PC=((ALOG(PHIC(NC)/PHI0)*(SGAM-GAM)/C)+SGAM*ZZ(NC)+P0)/(1.0E+05)
      TEMPC=TGRAD*ZZ(NC)+T0
C     IF(ZZ(NC).GT.2500.) TEMPC=TGRAD2*(ZZ(NC)-2500.)+TGRAD*2500.+T0
C
C     CHECK TO MAKE PRINTOUT OR NOT
C
      IF(QUIT.GT.0.) GO TO 12
      PT=TIMINC*PRINT
      IF(TT.LT.PT) GO TO 11
C
C     VARIABLES CONSTANT FOR ALL Z EVALUATED AT THIS TIME STEP
C
      TTK=TK/COR
   12 WRITE(4,1000) NAME
      WRITE(4,1005)
      WRITE(4,1010) PRINT,QUIT,DZ,TTP,TTK,NODES
      SUBR=(H-HC)/TK
      WRITE(4,1015) SEDR,SUBR,NFS,H
      WRITE(4,1020) TSED,TSUB,TFS,THS
      WRITE(4,1005)
C
C     FLUID AND MATERIAL PROPERTIES GIVEN FOR EACH NODE AT TT
C
      WRITE(4,1025)
      DO 10 J=1,NODES
      PHIE=PHI0*EXP(-C*Z(J))
      YLAM=P(J)/PL(J)
      PERM(J)=PERM(J)/(9.869E-16)
      WRITE(4,1030) J,Z(J),DWIDE(J),PHI(J),PHIE,PERM(J),YLAM
   10 CONTINUE
      WRITE(4,1005)
C
C     PRESS AND TEMP PARAMETERS GIVEN FOR EACH NODE AT TT
C
      WRITE(4,1035)
      DO 2 J=1,NODES
      TEMP(J)=TGRAD*Z(J)+T0
```

```
      IF(Z(J).GT.2500.) TEMP(J)=TGRAD2*DZ+TEMP(J-1)
      P(J)=P(J)/(1.0E 05)
      PH(J)=PH(J)/(1.0E+05)
      PL(J)=PL(J)/(1.0E+05)
      PEX(J)=PEX(J)/(1.0E+05)
      WRITE(4,1040) J,Z(J),PEX(J),P(J),PH(J),PL(J),TEMP(J),VEL(J),VR(J)
    2 CONTINUE
      WRITE(4,1005)
      WRITE(4,1055) NC,ZZ(NC),PHIC(NC),TEMPC,PC
      WRITE(4,1005)
C
C     PARAMETERS TO BE PLOTTED VERSUS DEPTH AT A PARTICULAR
C     TIME STEP
C
      WRITE(8,1050) NODES,TTP,TSED
      DO 3 J=1,NODES
      PHIE=PHI0*EXP(-C*Z(J))
      WRITE(8,1065) Z(J),PHI(J),PHIE,PL(J),P(J),PH(J),TEMP(J)
    3 CONTINUE
    4 CONTINUE
      PRINT= PRINT + 1.0
   11 CONTINUE
C
C     RECORD PROPERTIES OF NODE INTO GPTIME PLOT
C
      TTP=TTP/(1.0E+06)
      WRITE(9,1060) TTP,ZZ(NC),PHIC(NC),TEMPC,PC
      PRMAX=PRMAX+1.1
      RETURN
C
C     FORMAT STATEMENTS FOR SUBROUTINE OUTPUT
C
 1000 FORMAT(//////10X,1H*,80A1)
 1005 FORMAT(10X,117(1H=)/)
 1010 FORMAT(14X,8HPRINTOUT,5X,5HQUIT ,8X,3HDZ ,6X,10HTOTAL TIME,3X,9HTI
     .ME STEP,3X,5HNODES//10X,2(5X,I5),4X,E10.3,3X,2(2X,E10.3),3X,I5/)
 1015 FORMAT(15X,9HSED RATE ,3X,10HSUBS RATE ,3X,10HNUMBER: FS,
     .2X,17HDEPTH:  BASE (H) //14X,E10.3,2X,E10.3,3X,
     .1(I10,3X),7X,E10.3/)
 1020 FORMAT(15X,10HTOTAL SED ,2X,10HTOTAL SUBS,4X,9HTOTAL FS ,4X,9HTOTA
     .L HS ,5X,21H(ALL VALUES SINCE T0)//14X,4(E10.3,3X)/)
 1025 FORMAT(/11X,5HNODE ,4X,8HDEPTH   ,4X,8HDWIDE   ,2X,9HPOROSITY ,3X,
     .9HEQUIL POR,2X,12HPERMEABILITY,3X,6HLAMBDA/)
 1030 FORMAT(10X,I5,6(2X(E10.3)))
 1035 FORMAT(/11X,5HNODE ,4X,8HDEPTH   ,2X,10HPRESS: EX ,4X,8HPRESS   ,2
     .X,9HPRESS: HS ,3X,9HPRESS: LS ,
     .4X,8H TEMP   ,4X,7HFL VEL ,4X,10HSOLID VEL /)
 1040 FORMAT(10X,I5,2X,8(E10.3,2X))
 1045 FORMAT(6(E10.3))
 1065 FORMAT(7(E10.3))
 1050 FORMAT(I5,2E10.3)
 1055 FORMAT(10X,5HNODE:,I5,3X,8HDEPTH:  ,E10.3,3X,11HPOROSITY:  ,E10.3,
     .3X,7HTEMP:  ,E10.3,3X,8HPRESS:  ,E10.3/)
 1060 FORMAT(5E10.3)
      END
```

APPENDIX V

Application of Finite Difference Scheme

Expanding equation (7),

$$B_1\phi_z + B_2[b(\phi_z/\phi)^2 + (a - b/\phi)\phi_{zz}] = [\phi_t + v_r\phi_z]/(1-\phi) \quad . \qquad (V.1)$$

Solving for ϕ_t:

$$\phi_t = -v_r\phi_z + (1-\phi)\phi_z[B_1 + B_2b\phi_z/(\phi)^2] + B_2(1-\phi)[a - b/\phi]\phi_{zz} \quad . \qquad (V.2)$$

and

$$\phi_t = [B_1(1-\phi) + B_2b(1-\phi)\phi_z/\phi^2 - v_r]\phi_z + B_2(1-\phi)[a - b/\phi]\phi_{zz} \quad . \qquad (V.3)$$

Upon discretization, the following backward differences in time and center differences in space were taken:

$$[\phi_{i,j+1} - \phi_{ij}]\Delta t = \{B_1(1-\phi_{ij}) + B_2b(1-\phi_{ij})[\phi_{i+1,j} - \phi_{i-1,j}]/2\Delta z\phi_{ij}^2 - v_{r_{ij}}\}$$
$$[\phi_{i+1,j+1} - \phi_{i-1,j+1}]/2\Delta z + B_2(1-\phi_{ij})[a - b/\phi_{ij}]$$
$$\{\phi_{i+1,j+1} - 2\phi_{i,j+1} + \phi_{i-1,j+1}\}/\Delta z^2 \quad . \qquad (V.4)$$

Note which variables represent those of the present (i+1) or previous (i) timestep. Equation (V.4) can be expressed by the following:

$$\phi_{ij} = (\eta_1 + \eta_2)\phi_{i+1,j+1} + (1 - 2\eta_2)\phi_{i,j+1} + (\eta_2 - \eta_1)\phi_{i-1,j+1} \quad , \qquad (V.5)$$

where

$$\eta_1 = \Delta t\{B_1(\phi_{ij} - 1) + B_2 b(\phi_{ij}-1)[\phi_{i+1,j} - \phi_{i-1,j}]/2\Delta z\phi_{ij}^2 + v_{r_{ij}}\}2\Delta z$$

and

$$\eta_2 = B_2\Delta t(\phi_{ij} - 1)[a - b/\phi_{ij}]/\Delta z^2 \quad .$$

In matrix form equation (V.5) is:

$$\begin{bmatrix} (1-2\eta_2) & (\eta_1+\eta_2) & 0 & & \\ (\eta_2-\eta_1) & (1-2\eta_2) & (\eta_1+\eta_2) & & \\ & \ddots & \ddots & \ddots & \\ & & (\eta_2-\eta_1) & (1-2\eta_2) & \end{bmatrix} \begin{bmatrix} \phi_{1,j+1} \\ \phi_{2,j+1} \\ \vdots \\ \phi_{m-1,j+1} \end{bmatrix} = \begin{bmatrix} \phi_{1,j} \\ \phi_{2,j} \\ \vdots \\ \phi_{m-1,j} \end{bmatrix} + \begin{bmatrix} (\eta_1-\eta_2)\phi_0 \\ 0 \\ \vdots \\ -(\eta_1+\eta_2)\phi_{mj} \end{bmatrix}$$

where $m = h/\Delta z$ and $\phi_{mj} = \phi(h,t)$. Using backward differences in time, discretization of v_r and $h'(t)$ (equations (8) and (10)) results in:

$$v_{r_{ij+1}} = [s'_{j+1}(1-\phi_0) + \Sigma_1^{i\Delta z} \Delta z(\phi_{ij+1} - \phi_{i,j}/\Delta t]/(1-\phi_{ij+1}) \qquad (V.6)$$

and

$$h_{ij+1} = h_{i,j} + [\Delta t s'_{j+1}(1-\phi_0) + \Sigma_1^m \Delta z(\phi_{ij+1}-\phi_{i,j})]/(1-\phi_{m,j+1}) \quad . \qquad (V.7)$$

APPENDIX VI

Derivation of How a Sedimentary Package Compacts Through Time

The compaction of a sedimentary package can be followed through time by simply comparing its present porosity with the previous value every timestep. The amount of compaction of a sedimentary column can be calculated by documenting the compaction of each contained sedimentary packet. Initially the sedimentary package is of thickness (ℓ) such that:

$$\phi\ell = \ell_w \quad . \tag{VI.1}$$

If the porosity changed over a Δt, the new ϕ, or ϕ', would be given by:

$$\phi' = \phi + \Delta\phi \tag{VI.2}$$

or

$$\phi'\ell' = \ell_w' \tag{VI.3}$$

where

$$\ell_w' = \ell_w + \Delta\ell_w \quad . \tag{VI.4}$$

and

$$\ell' = \ell + \Delta\ell \quad . \tag{VI.5}$$

Because solid particles are conserved, $\Delta\ell_w = \Delta\ell$.

Substituting equations (VI.4) and (VI.5) into (VI.3):

$$\phi'(\ell + \Delta\ell) = \ell_w + \Delta\ell \qquad \text{(VI.6)}$$

and rearranging

$$\Delta\ell = \ell_w - \phi'\ell/(\phi'-1) \quad . \qquad \text{(VI.7)}$$

Upon eliminating ℓ_w,

$$\Delta\ell = \phi\ell - \phi'\ell/(\phi'-1) = -\ell(\phi' - \phi)/(\phi'-1) \quad . \qquad \text{(VI.8)}$$

Thus, $\Delta\ell$ gives how much the sediment compacted or expanded in the amount of time Δt.

The vita has been removed from the scanned document

A Numerical Compaction Model of Overpressuring in Shales

by

Laura A. Keith

(ABSTRACT)

A one-dimensional, numerical model of sediment compaction has been developed using porosity, velocity of sediment particles, and depth of the evolving basin as master variables. The governing set of nonlinear, partial differential equations are solved by a finite difference scheme devised to be stable for calculations involving tens of millions years and depths up to 4 km. Input parameters include a sedimentation function and a permeability-porosity function representative of the modeled sediment. Additional terms can be incorporated to mimic the effect of fluid volume generated by dehydration from clay mineral transformations and by temperature and pressure variations. Evolution of pressure, porosity, permeability, and fluid and sediment particle velocities are documented in a vertical sediment column as well as properties of a sedimentary package being successively buried.

Although this model has many potential applications, it is used here to demonstrate that the major cause of overpressuring in sediments accumulating along passive margins is nonequilibrium compaction. In general, smectite dehydration and aquathermal pressuring play minor roles in the development and sustenance of

overpressuring. Comparison of model cases and Gulf Coast overpressured cases shows that sedimention rates and strata permeability are the most important geologic factors in the formation of overpressured zones.